DOE/ER/53225--T8

DE93 002642

PROGRESS REPORT

"APPLICATIONS OF COMPUTER MODELING TO FUSION RESEARCH"

DEPARTMENT OF ENERGY GRANT NO. DE-FG03-86-ER53223, Task VIB

Grant Period 1988 - 1989

Principal Investigator: Prof. John M. Dawson

INTRODUCTION

Last year (1988), the Office of Magnetic Fusion of the DOE approved a Grant for a program on "Applications of Computer Modeling to Fusion Research" at UCLA. This Grant was provisionally approved for three years. The first year of this grant has been very productive and we propose that the second year of this grant be funded. This proposal contains a progress report for 88-89 and a list of publications and papers presented at meetings.

The major thrust of the program are to pursue a vigorous program of the development and application of Gyrokinetic Particle Codes to Tokamak Transport; development of Techniques to Take Advantage of Parallel Computers; Model Dynamo and Bootstrap Current Drive; and in general maintain our broad-based program in Basic Plasma Physics and Computer Modeling.

I. Progress In 1988-89

1). Three Dimensional Gyrokinetic Tokamak Code

Here we report the progress made during the past year in the areas of applications of gyrokinetic plasma simulation models for tokamak transport.

(i) Particle Code Development

We have undertaken to develop three dimensional electrostatic and magnetostatic gyrokinetic plasma simulation models and apply them to problems of anomalous transport due to microinstabilities as well as interaction of energetic particles with low frequency MHD modes. In collaboration with PPPL (W. Lee and T.S. Hahm) and IPP, Nagoya University, Japan (H. Naitou and T. Kamimura), we have made significant progress in the development of the algorithm and application of the model over the past year. The simulation code follows the guiding center motion of several hundred thousand particles in their self-consistent electric and magnetic fields with appropriate gyrophase averaging in order to include the FLR effects. Wave-particle resonances are naturally retained since exact particle motion along the magnetic field is followed. This is important in the high temperature regime of tokamak operation since ion and electron Landau damping are important dissipation mechanisms. Listed are the recent developments and improvements in the algorithms:

a) Extension of our three dimensional electrostatic slab model to a bounded cylindrical model with square cross section has been made. Inclusion of the curvature, gradient-B drifts and magnetic mirroring effect in the parallel equation of motion in the particle pusher. We have carried out studies to verify that the code gives the correct particle drift motion in model tokamak magnetic fields, valid in the large aspect ratio limit; i.e., we see the correct banana orbits.

b) The addition of the induction electric field as well as the perpendicular magnetic field perturbations due to parallel currents has also been

completed. The simulation code accurately produces the shear Alfven wave dispersion and the fluctuation energy per mode obeys the correct thermal equipartition law. Two separate algorithms have been implemented - one using a direct solution of the induction electric field (Vz - E) and the other using the canonical momentum (P_Z) and solving for the vector potential (A).

c) Electron-ion collisions using an energy-conserving, Monte-Carlo pitch angle scattering method, has been introduced and is shown to produce a Spitzer-like resistivity with correct temperature dependence. Further improvements have been made in the algorithm in order to improve its efficiency without loss of energy conservation or numerical stability properties. These improvements have resulted from a collaboration with LLNL (B. Cohen and T. Williams) and are as follows:

d) Inclusion of electron subcycling which is possible because of the disparate time scales between electrons and ions. Implementation into a two dimensional gyrokinetic code has shown we can gain a factor of three in speed up of the simulation runs, pushing the electrons nine times as often as the ions.

e) Vectorization of the particle charge assignment to the mesh and force assignment on the particle has been under development on the Cray-2 and another factor of two is possible in the run times.

(ii) Physics Problems Currently Under Investigation

A number of problems are now being attacked and preliminary results show that a number of interesting regimes in anomalous transport can be studied:

a) Ion Temperature Gradient Driven Turbulence

The saturation of the energy confinement time with increasing density and increase in the ion thermal conduction channel is conjectured to be a result of the ion temperature gradient driven modes. We have obtained results of the saturation amplitudes and wavenumber dependence of the electrostatic fluctuations as well as

the resultant ion thermal diffusivity using the three-dimensional electrostatic slab model. The value of the diffusivity and shape of the fluctuation spectra compare well with some of the TEXT measurements using laser scattering methods.

b) Collisionless and Collisional Trapped Electron Mode

We have made simulations with the bounded cylindrical model in order to study the heat and particle diffusion resulting from the trapped particle modes. A model tokamak field is chosen in order to give rise to trapped particles and we have neglected toroidal curvature effects in the Poisson equation as a first approximation. We have shown that the correct linear growth of the modes can be simulated and the runs are being extended into the nonlinear regime with many more modes included in the simulation.

c) Internal Kink Modes

The codes with the induction electric field are able to investigate current driven ideal MHD type modes. Using the cylindrical model with a current profile such that $q < 1$ on axis, we have been able to obtain the correct linear growth rate of the internal kink mode. This is important because it allows us to study the regime where reduced MHD is valid with addition of wave-particle effects.

2). Simulation of Bootstrap and Dynamo Currents in Tokamaks

We have been modeling dynamo and bootstrap currents which can be generated by plasma flows in Tokamaks. We use a 2-1/2 D model which is fully electromagnetic; the model includes the effects of toroidal field gradients and a vertical magnetic field. During the last year we have improved the model in a number of ways. We have replaced the periodic boundary conditions in the field solver with conducting boundary conditions; we have introduced a Monte Carlo collision operator in the particle pusher.

To date we have investigated only transient conditions. We introduce a neutral plasma cloud in the high field region. The cloud is expelled outward and in doing so

crosses the vertical magnetic field; this generates a current in the z direction (equivalent to a toroidal current in a Tokamak). The z current crossed with the vertical magnetic field ultimately establishes a plasma equilibrium. The z current is large enough to form closed magnetic surfaces. We find that with collisions the z current can be larger than with out it; however, the collision rate we must use to see this effect is unrealistically large. We expect that with collisions and appropriate sources and sinks for plasma we will be able to study steady states.

3). Parallel Computing

Parallel Computation represents one of the most promising methods of obtaining the computing power needed to handle realistic three-dimensional plasma models. With this in mind we developed a new algorithm (in collaboration with P. C. Liewer of JPL) for implementing plasma particle-in-cell (PIC) simulation codes on parallel computers. The algorithm, called the universal concurrent PIC algorithm (UCPIC) has been used to implement an electrostatic PIC code on the 32-node JPL Mark III Hypercube parallel computer. This algorithm has lead to very efficient parallel implementation of a well-benchmarked one dimensional code; the parallelism that is achieved is close to 100%. The performance of the Mark III Hypercube is about twice that of the MFE Cray II for this problem; with the use of faster hardware and more nodes this power will increase. Similar impressive performance should be obtained with other particle codes (such as the gyrokinetic code) when properly coded for such a parallel computer.

4). Particle Simulation of ICRF-Edge Plasma Interaction

The edge plasma region in Tokamaks plays an important role in the overall plasma confinement, particularly in H-mode discharges. Furthermore, when edge plasmas are 'driven', for example, when fast waves, lower hybrid or ion Bernstein waves are launched from an antenna structure nonlinear effects can produce particle acceleration, and hence impurity release when these particles interact with

the limiter. Because of the generation of nonthermal distributions, particle simulations are a vital tool for the analysis of antenna plasma coupling problems. The development of good models for this study requires codes with multiple species, ionization and recombination as well as inclusion of wall sputtering. As a first step, we have studied the collective plasma behavior near the edge, in the large amplitude regime, when the plasma is strongly driven. We have used two dimensional electromagnetic particle codes with oscillating current sheets and dipole current sources, launching ion cyclotron waves into a uniform plasma slab. Pondermotive effects, surface wave heating and nonthermal electron distributions have been observed. Although the particle boundary conditions were only simple reflection methods the next step will be the inclusion of more realistic sources and sinks.

We have also used one and two-halves dimensional guiding center electron, full dynamic ion electrostatic particle codes for the study of AC-RF sheath formation near Faraday shields. These sheaths are capable of forming potentials which can spawn impurity's from these shields. From the simulations we have found sheath formation on scale lengths the order of the ion gyroradius and have demonstrated the RF-rectification effect leading to large particle fluxes into the shield, with energies capable of causing sputtering.

5). Vlasov Ion-Fluid Electron Model

We have used the Vlasov Ion-Fluid Electron Model we had developed to investigate waves (ion Bernstein waves) generated by energetic ions (either injected ions or fusion reaction products). We found waves at integral and half integral multiples of the energetic ion cyclotron frequency for energetic protons in a deuterium plasma or in a deuterium proton plasma. The spectra look very much like those observed on JET and TFTR.

6). Basic Plasma Studies

In connection with our University Mission of Training Students in Plasma Research we have maintained a strong basic plasma physics program. In this area we have carried out studies on dynamic Debye clouds in a magnetized two-dimensional plasma and on waves in a bounded magnetized plasma.

II. Publications

Journal and Conference Proceedings

1. B.S. Bauer and V.K. Decyk, "Making movies on a Macintosh Plus from CRAY Output," SDSC Gather/Scatter, Vol. 4, No. 11, p. 1 (1988).

2. F. Kazeminejad, R. Sydora, J.M. Dawson, J.N. Leboeuf, and F. Brunel, "A Hybrid Vlasov-Fluid Model of Kinetic Ions and Massless Fluid Electrons," J. Comput. Phys., submitted (1988).

3. Sydora, R.D., T.S. Hahm, W.W. Lee and J.M. Dawson, "Fluctuations and Transport Due to Ion Temperature Gradient-Driven Instabilities," submitted to Physical Review Letters, November 1988.

4. W.M. Tang, N.L. Brentz, T.S. Hahm, W.W. Lee, F.W. Perkins, M.H. Redi, G. Rewoldt, M.C. Zarnstorff, S.J. Zweben, R.D. Sydora, J.M. Dawson, V.K. Decyk, H. Naitou, T. Kamimura, and Y. Abe, "Theoretical Studies of Enhanced Confinement Properties in Tokamaks," PPPL-2580, January 1989; to appear in Plasma Physics and Controlled Nuclear Fusion Research, (IAEA; Nice, France, 1988).

5. P.C. Liewer, B.A. Zimmerman, V.K. Decyk, and J.M. Dawson, "Application of Hybercube Computers to Plasma Particle-In-Cell Simulation Codes," Proc. of 4th International Conference on Supercomputing, Santa Clara, CA (1989).

6. R.D. Sydora, "Application of Long Time Scale Plasma Simulation Methods Applied to the Problems of Anomalous Plasma Confimenemt," Proc. of 4th International Conference on Supercomputing, Santa Clara, CA (1989).

Conference and Workshop Presentations

30th Annual Meeting of the American Physical Society, Division of Plasma Physics, October 31 - November 4, 1988

1. "Simulations of Collisionless Coupling of Unstable Ion Distributions," R. Bingham, J.M. Dawson, F. Kazeminejad, and J.J. Su.

2. "Interaction of a Neutral Beam and an Ambient Plasma," F. Kazeminejad, R. Bingham, J.M. Dawson, and J.N. Leboeuf.

3. "Test Charges in 2D Plasma," V.K. Decyk, H.-C. Huang, and J.M. Dawson.

4. "Study of Kinetic Effects on MHD Modes Using A Three-Dimensional Gyrokinetic Plasma Simulation Model," R.D. Sydora, H. Naitou, W.W. Lee, T.S. Hahm, and J.M. Dawson.

5. "Theory and Simulation of the Magnetized Debye Cloud," H.-C. Huang, V.K. Decyk, and J.M. Dawson.

6. "Simulation of Transport Driven Current in Tokamaks," W.J. Nunan, R.D. Sydora, and J.M. Dawson.

7. "A Universal Concurrent Algorithm for Plasma Particle-In-Cell Simulation Codes," P.C. Liewer and V.K. Decyk.

Transport Task Force Meeting, January 11-13, 1989, Austin, TX

1. "Application of Gyrokinetic Plasma Simulation Methods to the Problem of Anomalous Transport Due to Microinstabilities," R. Sydora.

Workshop on ICRF Edge Physics, January 26-27, 1989, Boulder, CO

1. "Particle Simulation of Surface Wave Heating and Particle Acceleration in the Presence of RF in the Tokamak Edge Plasma," R. Sydora.

Fourth Conference on Hupercube Computers and Applications, March 1989, Monterey, CA

1. "A General Concurrent Algorithm for Plasma Particle-In-Cell Simulation Codes," V.K. Decyk, J.M. Dawson, P.C. Liewer, E.W. Leaver, and G.C. Fox.

1989 Sherwood Theory Conference, Annual Controlled Fusion Theory Conference, April 3-5, 1989, San Antonio, TX

1. "Computer Simulation of Transport Driven Current Tokamaks," W.J. Nunan, R.D. Sydora, and J.M. Dawson.

2. "Particle Simulations with Predictive Dynamic Load balancing on Hypercube and Ncube Multiprocessors," R.W. Huff and J.M. Dawson.

3. "Three Dimensional Gyrokinetic Plasma Simulation Models for the Study of Low Frequency Microinstabilities," R.D. Sydora, H. Naitou, W.W. Lee, J.M. Dawson, and T.S. Hahm.

4. "Simulation of the Ion Cyclotron Emission in the JET Tokamak," F. Kazeminejad, R. Bingham, J.M. Dawson, and J.N. Leboeuf.

Plasma and Fusion Society Meeting, April 1989, Japan

1. "Plasma Simulation by Using 3-D Gyrokinetic Particle Code," H. Naitou, Y. Abe, T. Kamimura, R.D. Sydora, V.K. Decyk, J.M. Dawson, W.W. Lee, and T.S. Hahm.

2. "MHD Simulation Using 3-D Gyrokinetic Particle Code," H. Naitou, Y. Abe, T. Kamimura, R.D. Sydora, V.K. Decyk, J.M. Dawson, W.W. Lee, and T.S. Hahm.

Thesis

1. "Theory and Simulation of the Test Particle Debye Cloud," H.-C. Huang.

2. "Simulation Study of Surface and Body Waves in a Magnetized Bounded Plasma," D. Sultana.

3. "Hybrid Modeling of Plasmas and Applications to Fusion and Space Physics," F. Kazeminejad.

DOE/ER/53225-T8

TASK IIIA

SECTION I: PROGRESS REPORT FY89

I. INTRODUCTION

The purpose of the Task IIIA program at UCLA is to develop innovative systems capable of providing the detailed diagnostic information essential to the success of the fusion program, while the associated Task IIIB program is concerned with the development of advanced technology and concepts required to elucidate critical physics issues. In undertaking this work, the philosophy has always been that the development program should not be carried out in isolation, but respond to the needs of the fusion community in general, and in particular to those of the mainline devices, TFTR, DIII-D and CIT. Examples of this work include the development of mixers for the TFTR ECE and interferometry systems, the design of the MTX FIR interferometer/polarimeter system, and the DIII-D 1 mm scattering system.

Another major goal of the UCLA program has always been the dissemination of the diagnostic expertise and technology developed under Task IIIA, both through publication and collaborative projects. This aspect of the program has continued to experience exceptional success during the last year with many collaborative projects completed, initiated, or under discussion. These include the DIII-D systems mentioned above, the MTX high resolution FIR interferometer/polarimeter system, high power optically pumped FIR laser requests from Los Alamos National Laboratory and the UKAEA Culham Laboratory, as well as possible involvement in the Wisconsin MST device. This high level of interest in collaboration with UCLA is indicative of the quality of the work performed under Task's IIIA and IIIB.

During the past year, the major effort conducted under the Task IIIA program has been the design, fabrication and testing of a proof-of-principle 1 mm scattering system for DIII-D which has recently begun operation. However, now that the system has demonstrated the ability to provide physics information, the scattering efforts will be transitioned out of the base program.

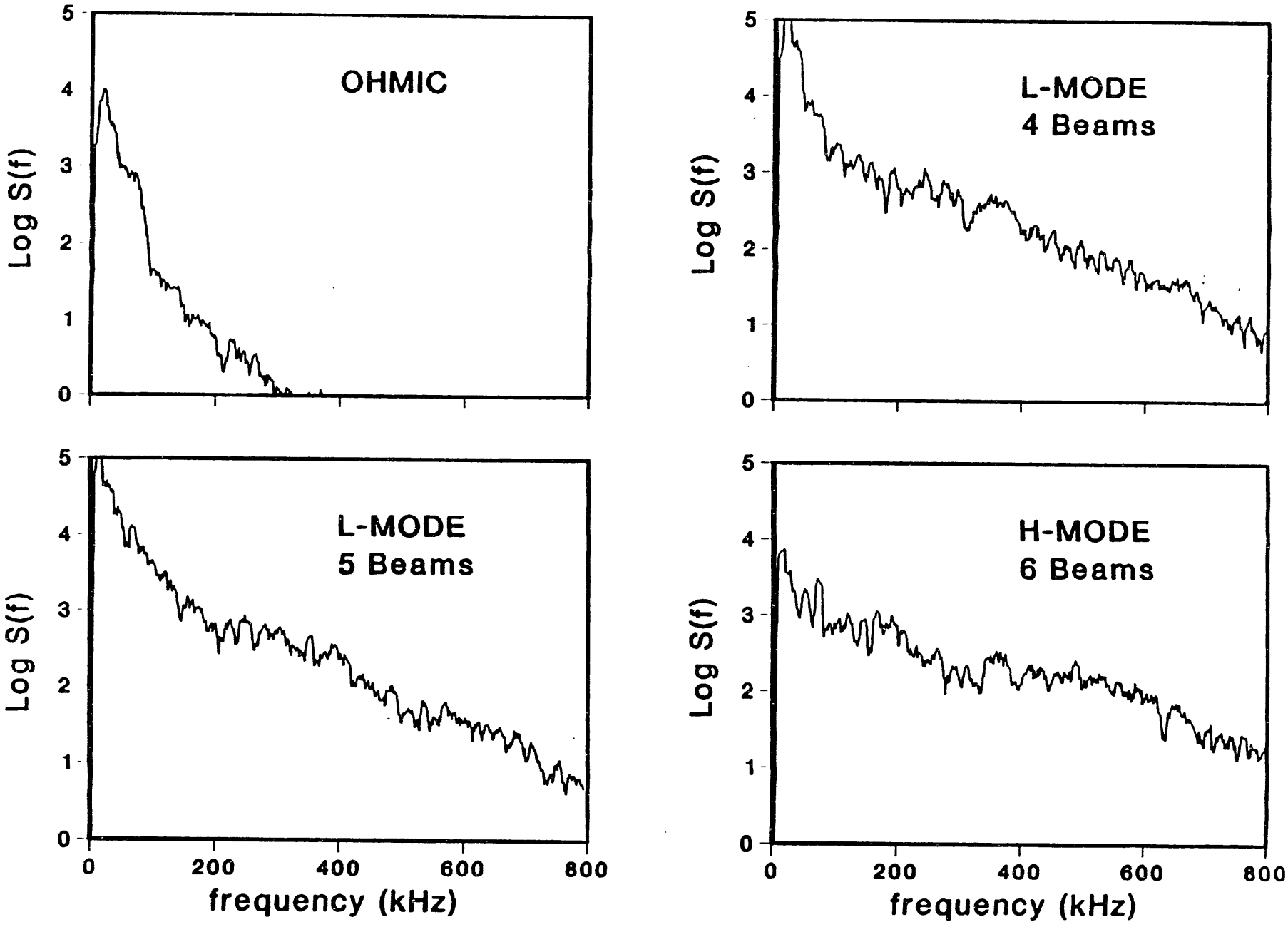
DENSITY FLUCTUATION SPECTRA [outer edge, K⊥= 12 1/cm]
OHMIC
L-MODE
4 Beams
L-MODE
5 Beams
H-MODE
6 Beams
Log S(f)
frequency (kHz)
0
1
2
3
4
5
200
400
600
800

Figure 8

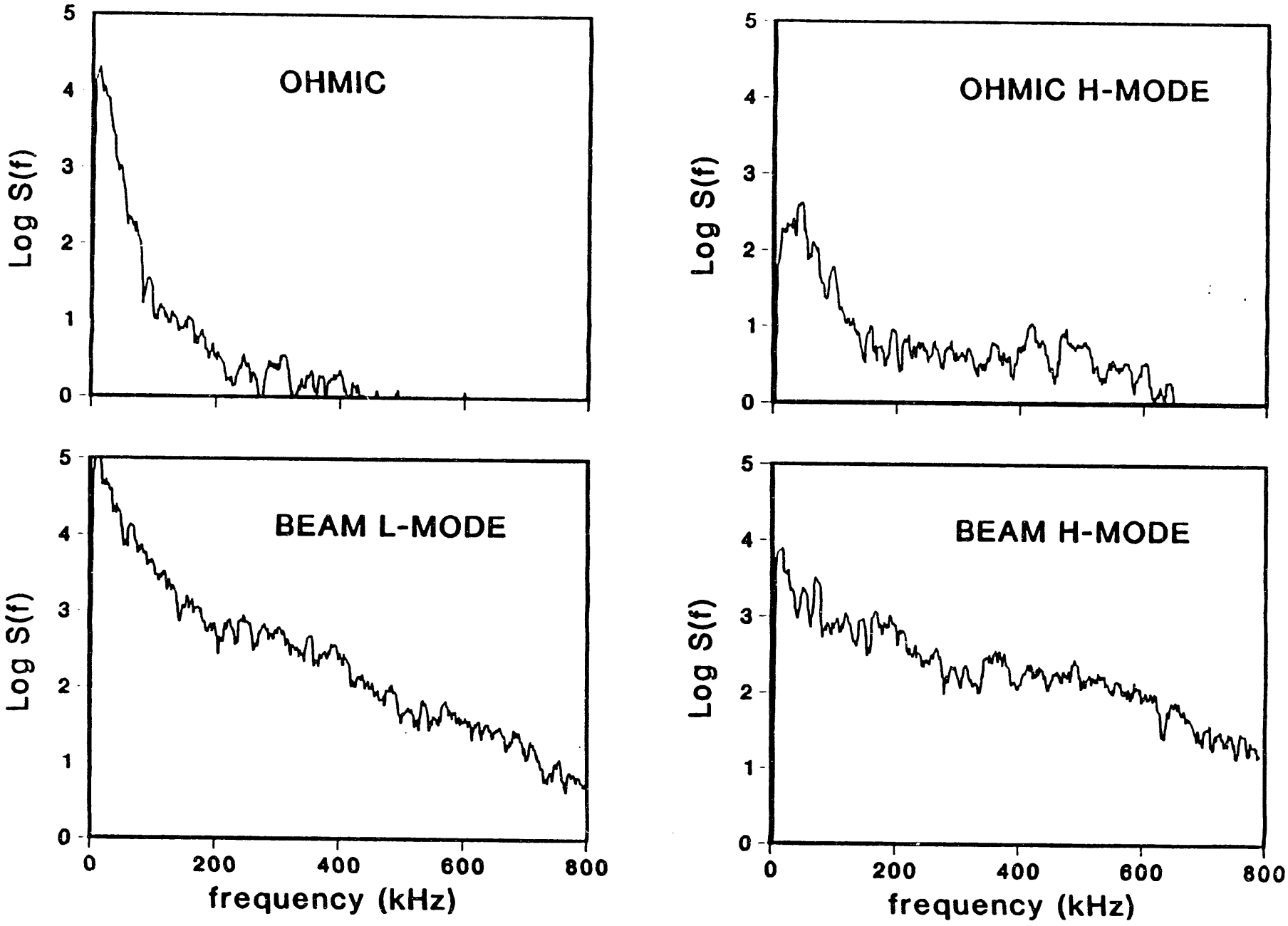
DENSITY FLUCTUATION SPECTRA [outer edge, K⊥= 12 1/cm]
OHMIC
OHMIC H-MODE
BEAM L-MODE
BEAM H-MODE
Log S(f)
frequency (kHz)
0
1
2
3
4
5
0
200
400
600
800

Figure 9

Density Fluctuations OHMIC / L-MODE / L-MODE - H-MODE Tran

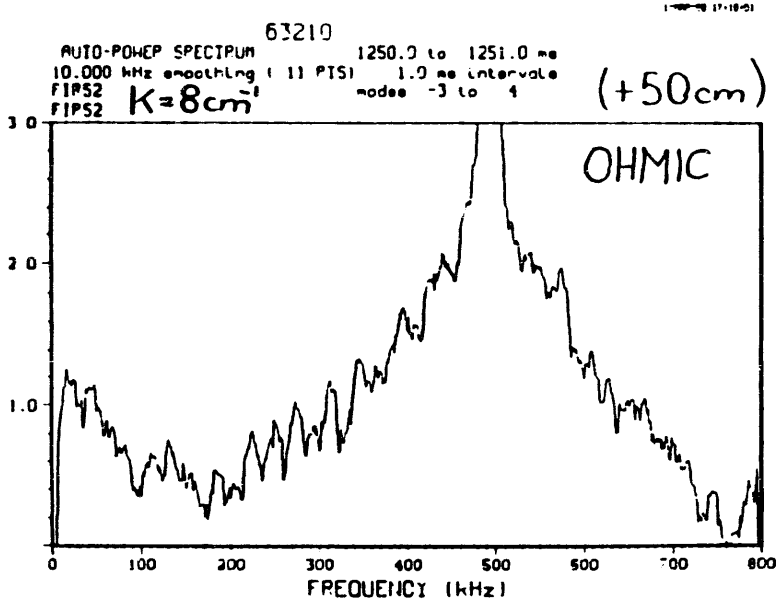

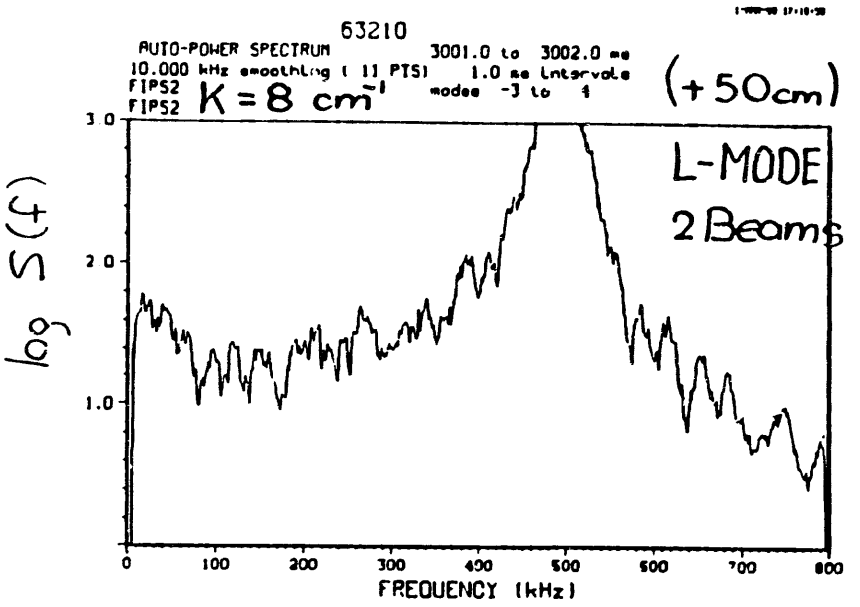

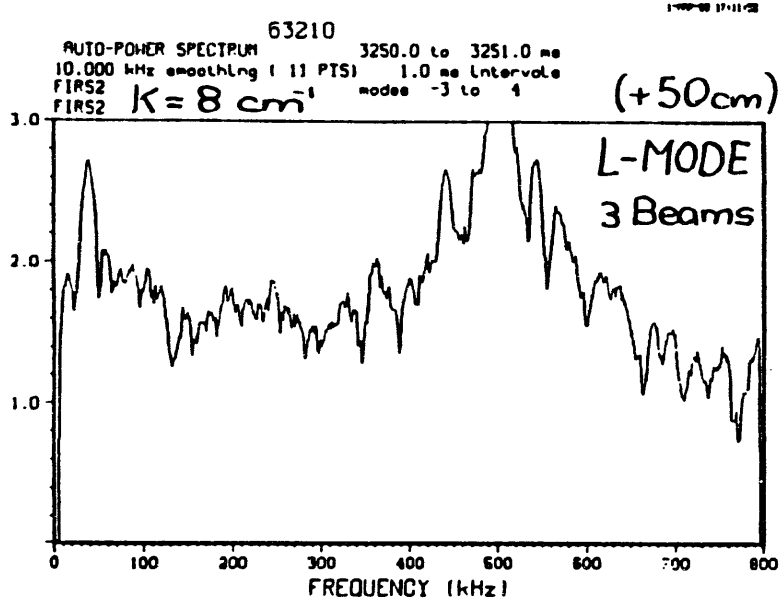

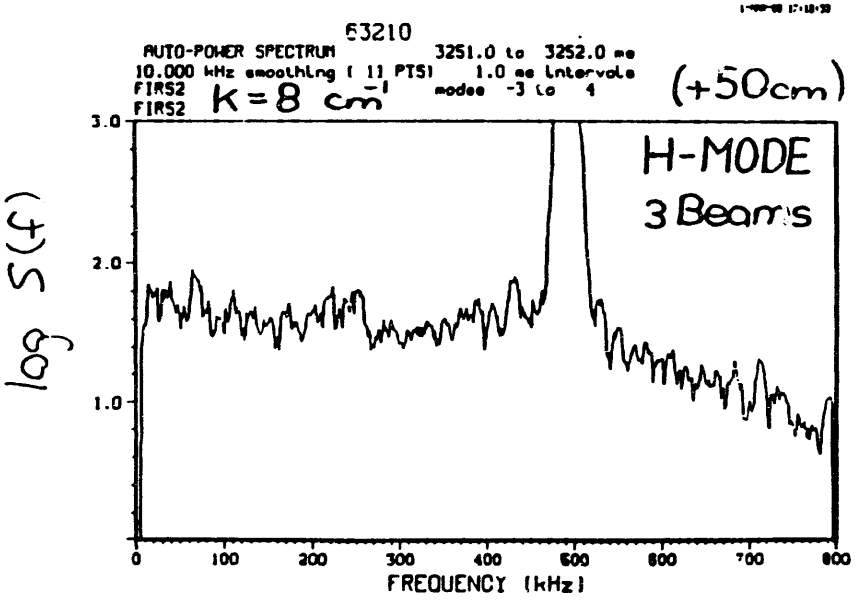

1 MA ; Divertor ; x - low ; Max. 3 Beams

Figure 10

II. PROGRESS

As mentioned above, the major portion of the Task IIIA efforts was directed toward the design, fabrication, installation and proof-of-principle operation of a 1 mm scattering system for DIII-D. The major impetus for this work was the UCLA scattering measurements on TEXT which identified a low frequency ion mode which appears to possess features consistent with the predictions of η_i mode theory. It is therefore essential to investigate the issue of whether such a mode can exist in H-mode plasmas which possess extremely flat density gradients in the interior as well as the important question of the role of microturbulence in the L to H-mode transition.

The actual scattering system uses a twin far infrared laser which is located about eight meters away from the DIII-D tokamak in a small laser laboratory behind the concrete shield wall. Radiation is becoming more and more of a concern on DIII-D since many experiments currently use deutrium neutral beam sources injected into deutrium plasmas. Having the FIR laser outside the closed tokamak pit area provides more flexibility in running the scattering experiment. Two overmoded dielectric waveguides (see Fig. 1), one for the probe beam and one for the local oscillator beam, run from the laser laboratory to an optical table which is located near the tokamak entry port assembly.

The port assembly is fixed to the R 0 port in the midplane of DIII-D at the 195° elevation (see Fig. 2). Fifteen centimeters above the midplane of the machine, the probe beam is directed horizontally into the tokamak and is reflected back onto itself from a special carbon tile. This carbon tile has been precisely aligned during a machine vent while calibrating the scattering geometry. A scattering mirror (see Fig. 3) inside the port assembly reflects the scattered radiation out of the machine through two twenty-five centimeter diameter fused quartz windows. The scattering mirror can be adjusted in angle between 32° and 40° by a mechanical feedthrough. Ray tracings of the scattered radiation are shown in Fig. 4, allowing scattering from different spatial locations into different scattering angles. These ray tracings have been cross checked by experiments with HeNe laser beams and geometrical calculations. Wave number values in the range between 2 and 24 cm^{-1} can be measured with a wave number resolution Δk of $\pm$ 0.7 cm^{-1}. Because of the relatively large probe beam size, spatial resolution is on the order of $\pm$ 20 cm at a k-value of 12 cm^{-1}. At very low scattering angles,

spatial resolution becomes rather poor and is essentially an integration over the entire plasma diameter. However, at k = 6 cm^{-1} measurements are still spatially resolved with respect to the inner and the outer midplane.

An optical table is fixed in the vertical plane close to the entry port assembly (see Fig. 5). Collecting mirrors fixed on translation and rotation stages reflect the scattered radiation to their respective detectors. In its final form, the experiment will have four detectors looking simultaneously at four different scattering angles or different scattering locations. A fifth detector is intended to be used as an interferometer channel.

Preliminary measurements and tests have been made with two scattering channels only. This results from the relatively low laser power which can be expected from the 1.22 mm laser line. On the other hand, the laser system provides heterodyne detection capability which is crucial in our experiment. Figure 6 shows the differences between a homodyne and a heterodyne detection system as well as some characteristics of the two proposed radiation sources. A relation between the scattering angle and the measured wave numbers given by the Bragg condition for expected wavenumbers in the DIII-D tokamak can be found in Fig. 7.

The first attempts to detect scattering signals were made during the last two weeks of DIII-D operation in 1988. Following initial data acquisition problems and alignment difficulties with the receiver optical system signals with good signal-to-range level were obtained in January.

Several other problems, however, subsequently required resolution. For example, problem appeared with the pulling of the 1 MHz intermediate frequency (IF) which is used in the heterodyne detection system and which is obtained from the mixing of the probe beam and the local oscillator beam. In fact, since the probe beam is precisely reflected onto itself from the inner wall of the tokamak, the path between the laser and the reflecting carbon tile acts as an outer laser cavity. Because of the change of the refractive index in this additional cavity during a plasma shot, the frequency of the probe beam is slightly changed. Since the local oscillator frequency stays constant the intermediate frequency is shifted. Shifts of up to 200 kHz have been measured and they vary strongly during the plasma discharge. By using the system in the homodyne detection mode this problem does not exist. We therefore performed some first measurements using only one laser cavity.

Some very interesting features could be observed during plasma discharges with additional neutral beam heating. Looking at a particular shot (see Fig.

8) at four distinct times during the discharge we observe clearly different frequency spectra. Early in the discharge, we have a pure ohmic plasma with no beams injected. We observe that the spectrum is narrow in frequency and the scattered power is small compared to the spectra in the L-mode phase where in addition tc the ohmic current four or five 1.5 MW of neutral beams have been injected. The frequency spectrum is now very broad and enhanced in power by at least one order of magnitude over the entire frequency range. An additional sixth beam, however, leads to a transition from the low confinement regime L-mode into the high confinement regime H-mode. We observe that the scattered power at the low frequency end drops by more than an order of magnitude while the high frequency part above 400 kHz is increased. The high confinement regime can also be reached in a pure ohmic plasma. It is worth noticing that between the transitions from ohmic to H-mode and from L-mode to H-mode, the changes of the frequency spectra are qualitatively very similar (see Fig. 9).

One attempt made to overcome the frequency pulling in the heterodyne detection mode, was to use a polarizing beamsplitter and a quarter wave plate in the probe beam. The quarter wave plate would convert the linear polarization of the probe beam into circular polarization. A double pass would reconvert the returning beam to linear polarization but rotate its polarity by 90°. The returning beam would then be rejected by the polarizer. Using this optical system, the frequency pulling could be reduced by a certain amount, but not completely eliminated. Another way to solve the problem is to tilt the probe beam in order to prevent the reflected beam from going back to the laser cavity. Although this is simple to do it leads to inconveniences in respect to the scattering geometry. Furthermore, refraction at high plasma density may deviate the beam back to its original position.

Heterodyne scattering measurements have been made during the last month using a slightly tilted probe beam. Scattering angles have been recalculated to allow for a probe beam pointed down by an angle of $-1.5°$. We again show frequency spectra observed during ohmic, L-mode and H-mode phases (see Fig. 10). The central peak at 500 kHz is due t the IF frequency. The parts of the spectra to the left of the IF are due to the electron term, or fluctuations propagating in the electron diamagnetic drift direction. The parts to the right f the spectra are due to fluctuations propagating in the ion diamagnetic drift direction. The measurements done with the homodyne system could be confirmed with the heterodyne system. The scattered power

is enhanced and extends over a much larger frequency range when neutral beams are injected into the plasma. It is interesting to observe in Fig. 10 that the lower two spectra are only separated by one millisecond. The L-mode to H-mode transition seem to be very fast and the change in the fluctuation level is certainly remarkable.

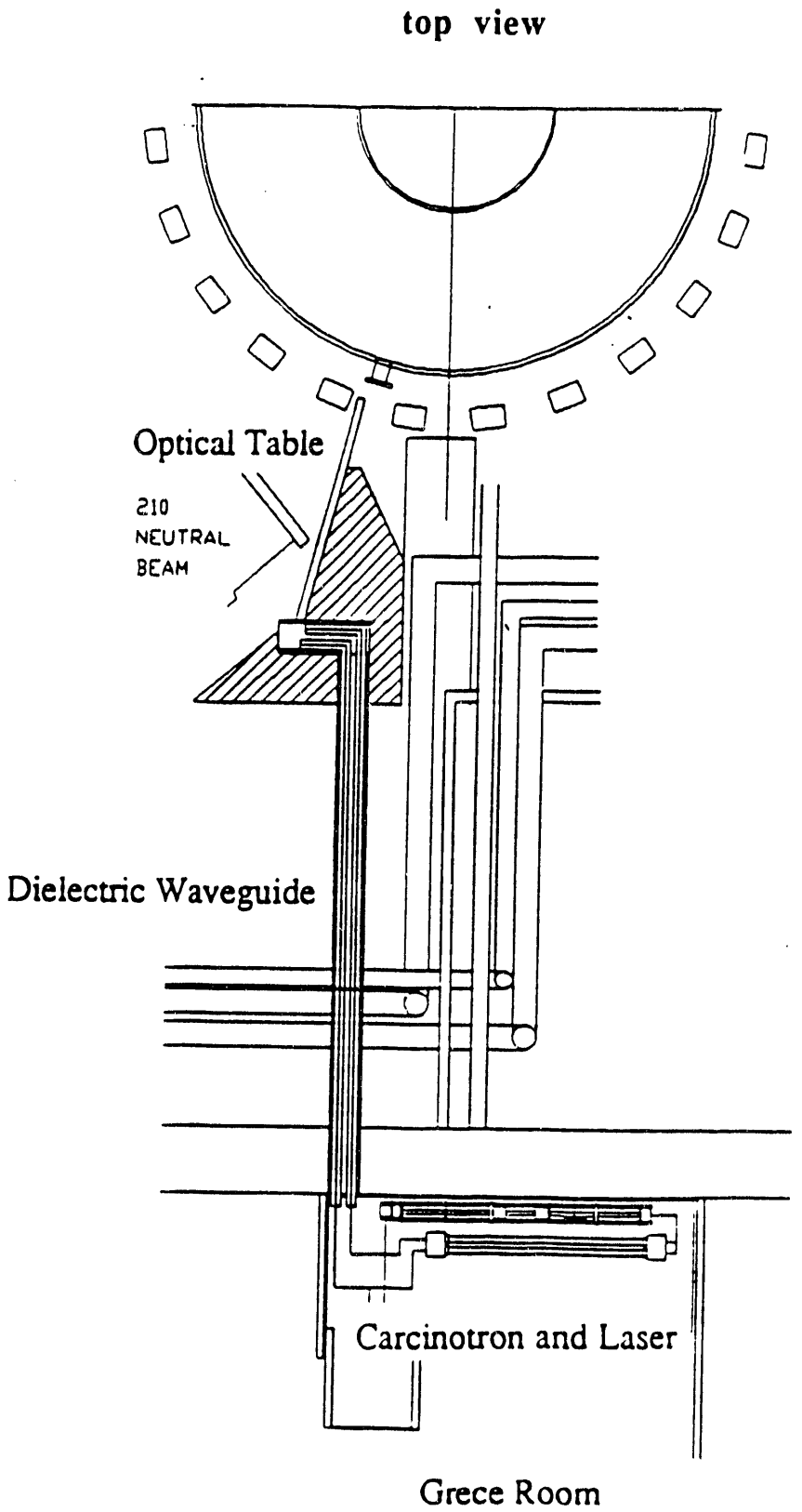

Figure 1 Layout of Scattering System - DIII-D Site.

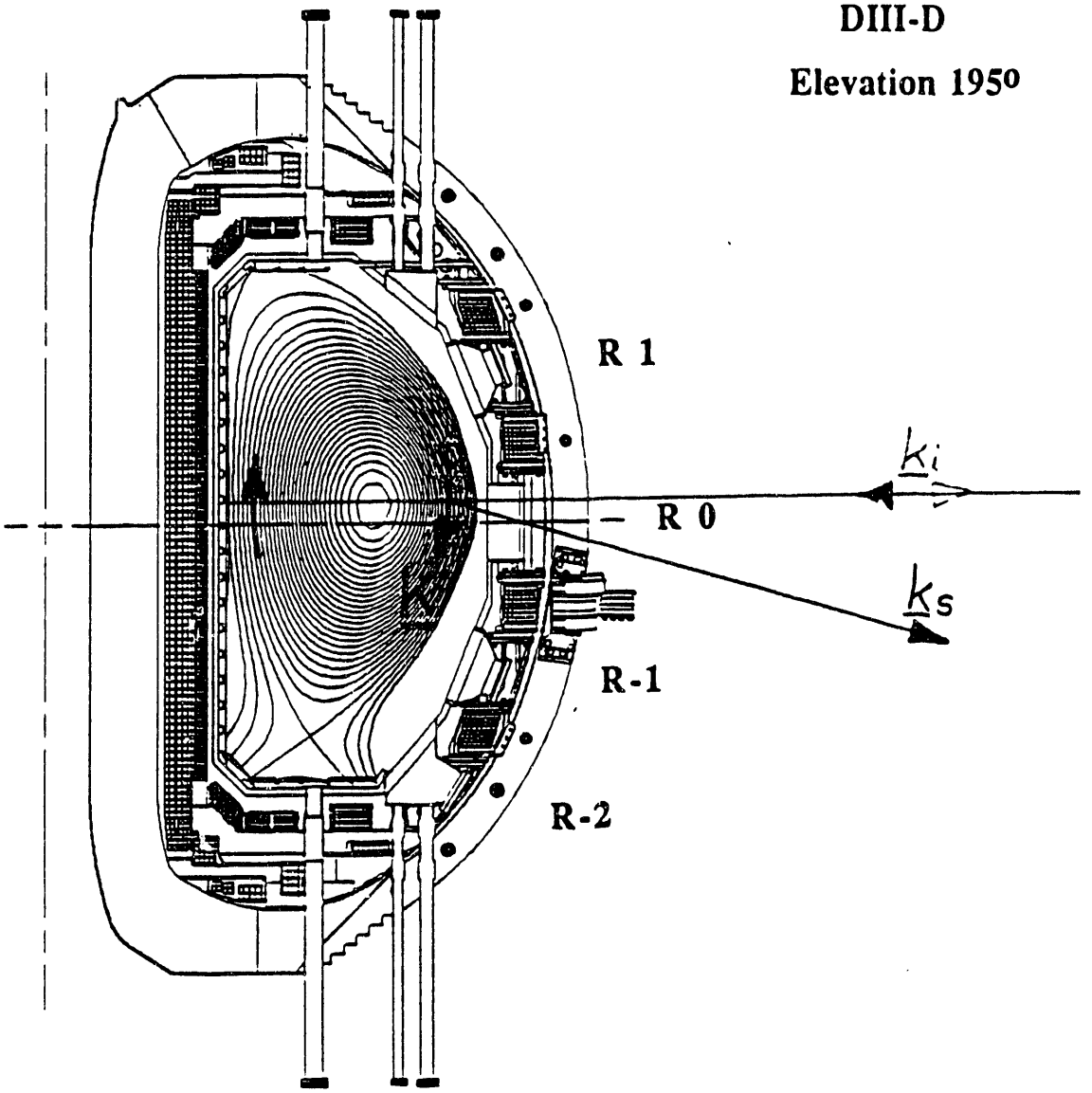

Major Radius	**R**	**= 1.67 m**
Minor Radius	**a**	**= 0.67 m**
Aspect Ratio	**A**	**= 2.5**
Elongation	**κ**	**= 2.1**

Figure 2 DIII-D Tokamak - Experimental Access.

SPATIAL RESOLUTION !

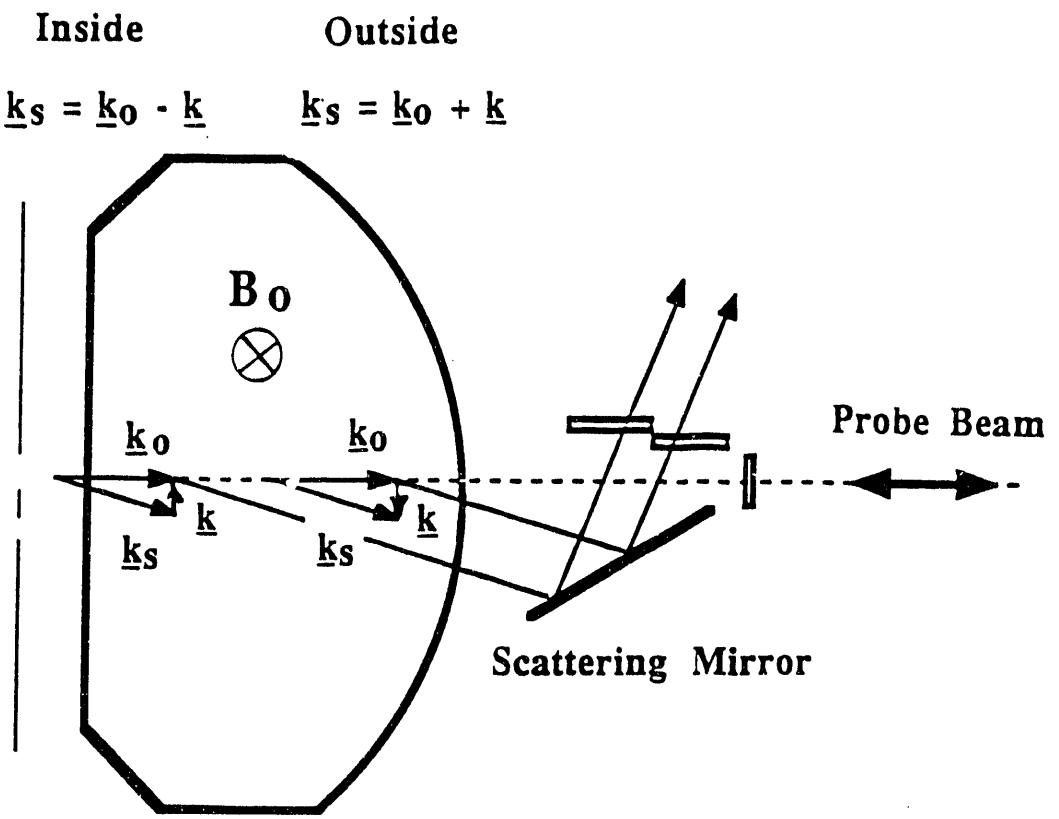

Bragg Law :	$K = 2\, k_0 \sin \Theta/2$
Probe Beam :	$\lambda_0 = 2\pi/k_0 \approx 1$ mm
Scattering Angles :	$2^o < \Theta < 24^o$
Wavenumber range :	$2 < K < 24$ cm^{-1}

Figure 3 Layout of Scattering System: - Entry Port.

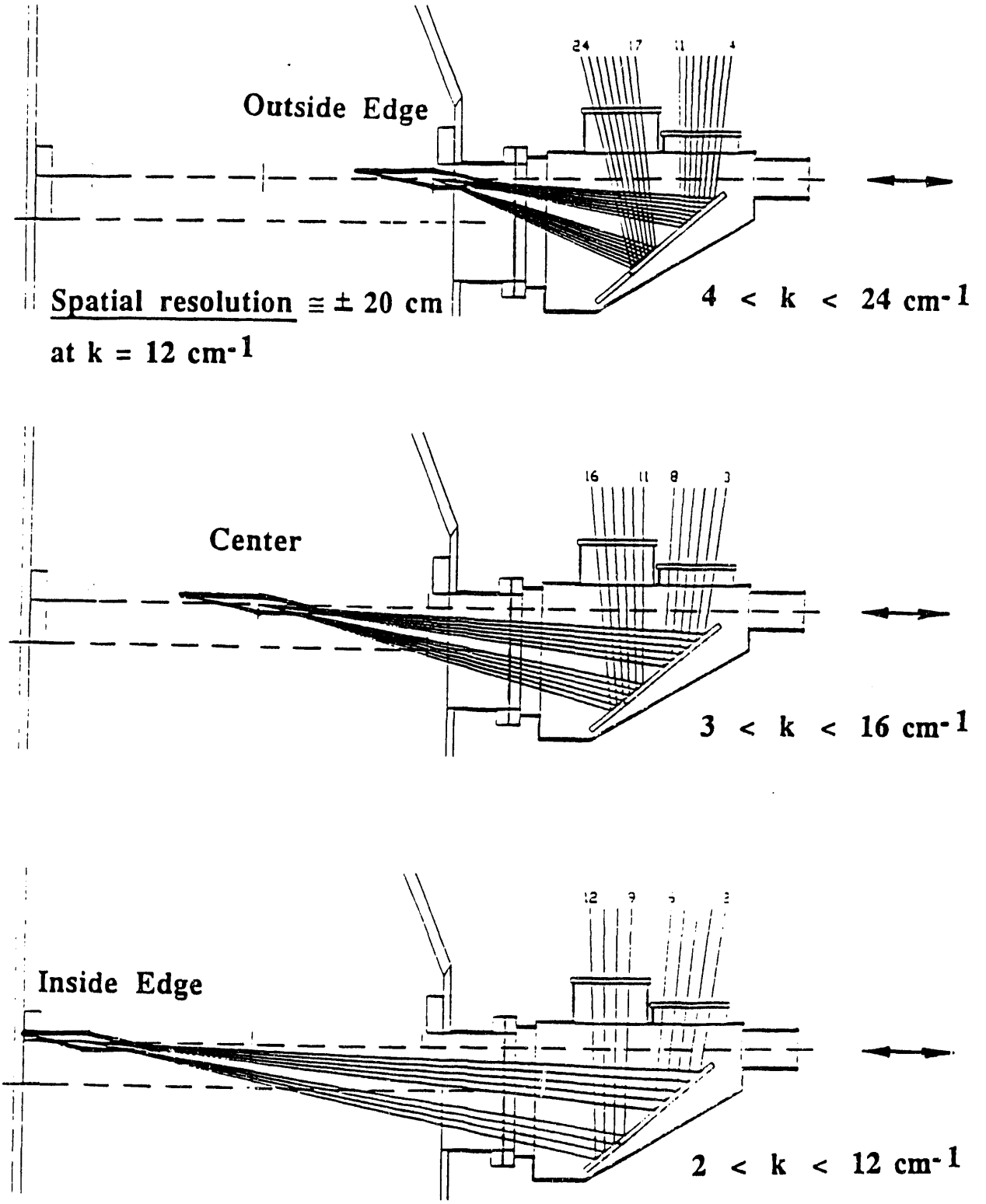

Figure 4 Layout of Scattering System - Entry Port.

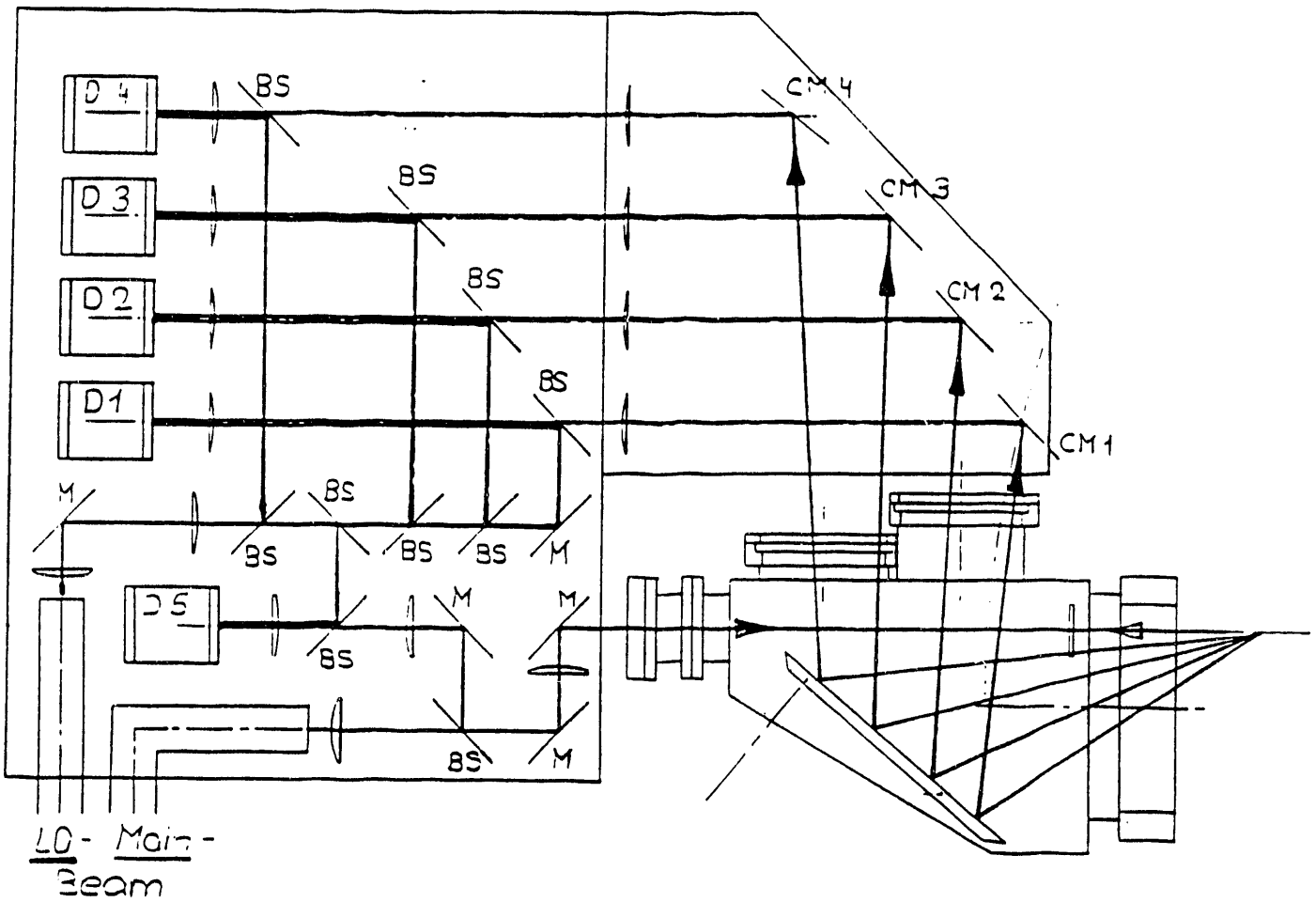

Detectors : **Waveguide mounted Schottky Barrier Diode Mixers / Preamplifiers / Linedrivers.**

Lenses: **High density Polyetylene.**

Beam Splitters: **Wire Meshes deposited on Mylar.**

Mirrors: **First surface Optical Mirrors.**

Figure 5 Layout of Scattering System: Detection Optics.

HETERODYNE DETECTION ! $\omega_0 \pm \omega$

homodyne

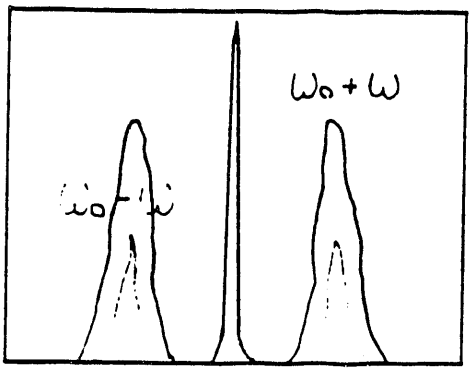

Ref

$\omega_{Lo} = \omega_0$

$\omega_S = \omega_0 \pm \omega$

heterodyne

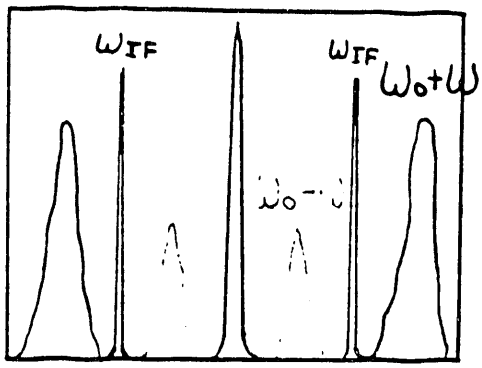

Ref

$\omega_{Lo} = \omega_0 \pm \omega_{IF}$

$\omega_S = \omega_0 \pm \omega$

Optically pumped Twin FIR Laser (1 Channel)

245 GHz ; $\lambda_0 = 1.22$ mm ; $P_0 \approx 10$ mW

Carcinotron and phase locked Klystron (4 Channel)

Probe Source CARCINOTRON:

280 GHz ; $\lambda_0 = 1.07$ mm ; $P_0 \approx 200$ mW

LO Source KLYSTRON:

tunable 140 GHZ Klystron, frequency doublet.

Figure 6 Layout of Scattering System: Radiation Sources.

K-VALUES MEASURED AT CORRESPONDING SCATTERING ANGLES

Scattering Angle	Radiation source	
	Laser 245 GHz λ_o= 1.22 mm	Carcinotron 290 GHz λ_o = 1.07 mm
θ [^{o}]	K [cm^{-1}]	K [cm^{-1}]
2	1.8	2.0
4	3.6	4.1
6	5.4	6.1
8	7.2	8.2
10	9.0	10.2
12	10.8	12.3
14	12.6	14.3
16	14.3	16.3
18	16.1	18.4

K - values of interest in DIII-D according to η_i mode condition $K_\perp \rho_i < 1$; $K < 9\ cm^{-1}$.

Figure 7 Layout of Scattering System: Radiation Sources.

TASK IIIB

SECTION I: PROGRESS REPORT FY89

I. CURRENT PROFILE MEASUREMENTS

Measurement of the current density profile in tokamak devices is of fundamental importance in understanding plasma stability and transport phenomena. Many techniques have been proposed to measure this parameter and have been attempted in proof-of-principle experiments with varying degrees of success. However, Faraday rotation continues to a particularly attractive technique for tokamaks operating over a wide range of densities and toroidal field values in contrast to a number of the approaches. It is well known that a plane electromagnetic wave, as it propagates through a plasma, will suffer changes in its polarization state through Faraday rotation ψ_p and elliptization ϵ_p. They are given respectively by

$$\psi_p(x) = 1.50\, x\, 10^{-20}\lambda^2 \int_o^L n_e(z) B_{PH}(z) dz \tag{1}$$

$$and\ \epsilon_p(x) = 6.43\, x\, 10^{-49}\lambda^5 B_T^2(x) \int_o^L n_e(z)\, dz \int_o^L n_e(z)\, B_{PH}(z) dz \tag{2}$$

where
- ψ_p: rotation angle in degree
- λ: probing wavelength in μm
- n_e: electron density in cm^{-3}
- B_{PH}: poloidal field component parallel to the probe beam in kG
- B_T: toroidal field in kG
- L: probing chord length in cm

Here, it is assumed that ω^2 is much larger than both ω_{pe}^2 and ω_{ce}^2. The most successful scheme for the detection of Faraday rotation is that pioneered by Soltwisch on the TEXTOR tokamak in which a phase-sensitive detection method has been used to measure the small amplitude variations caused by the Faraday rotation. The output signal of the scheme is related to the rotation angle and the elliptization as follows

$$R\, cos\Delta\phi = c\, \frac{\psi_p + \epsilon_p}{1 - \psi_p - \epsilon_p} \tag{3}$$

where R: the ratio of the polarimeter signal to the interferometer signal
$\Delta\phi$: the phase difference ($\phi_I - \phi_F$) between the polarimeter and interferometer signals

It can be seen that the scheme is quite sensitive to the elliptization ϵ_p.

The purpose of the present work is not only to establish a routine polarimetric measurement of the current density profile on TEXT, but also to extend the measurement to higher densities and fields, as well as the study of the modification of the current density profile during ECRH. Therefore the major emphasis has been on the investigation of the possibility of measuring both the Faraday rotation and elliptization of the incident electromagnetic wave in order to more accurately compensate for the expected large elliptization at submillimeter wavelength on devices such as MTX and CIT.

During the year, extensive concept and experimental studies have been performed to assess the feasibility of polarimeter systems to be installed on a number of devices and, to establish accuracy limitations. We have proposed and tested two detection schemes for polarimetry which are different from that of Soltwisch in using a small wire spacing polarizer as beam combiner. The schematic of the two interferometer/polarimetry system is shown in Fig. 1. Parabolic cylindrical mirrors are used to expand the probe and reference beams in one dimension to view the entire plasma cross section. The two beams are combined and detected using a linear array of corner cube GaAs Schottky barrier diode mixers. In the first detection scheme, the polarization change due to the plasma effect yields two output signals whose amplitude ratio is given by

$$R = \sqrt{\frac{(1+\epsilon_p^2) - (1-\epsilon_p^2) sin2\psi_p}{(1+\epsilon_p^2) sin2\psi_p}} \simeq cot(\psi_p + \frac{\pi}{4}) \; when \; \epsilon_p << 1 \qquad (4)$$

In addition, there is a phase difference between equivalent detectors given by

$$\Delta\phi = tan^{-1}\left[\epsilon_p tan(\psi_p + \frac{\pi}{4}\right] - tan^{-1}\left[\epsilon_p tan(\psi_p - \frac{pi}{4}\right] \qquad (5)$$

In a second detection scheme, a polarization transforming reflector (PTR) is used as a quarter-wave polarizer to rotate the polarization direction of probe beam by 45° and quadrature phase-sensitive detection technique is

used to measure the Faraday rotation and elliptization simultaneously, which are given as follows

$$R\,cos\Delta\phi = tan\phi_p \frac{1-\epsilon_p^2}{1+\epsilon_p^2 tan^p\phi_p} \simeq tan\phi_p \;\; when\; \epsilon_p << 1 \qquad (6)$$

$$R\,sin\Delta\phi = \epsilon_p \left[cos^2\phi_p(H\epsilon_p^2 tan^2\phi_p)\right]^{-1} \simeq \epsilon_p \;\; when\psi_p << 1 \qquad (7)$$

In principle, therefore, measurement of the amplitude ratio and phase difference or quadrature output from the phase-sensitive detection system, allows one to independently evaluate the Faraday rotation ψ_p and elliptization as ϵ_p. It should be noted that the Faraday rotation measurement with both our schemes is very insensitive to the elliptization compared to the Soltwisch scheme. Also, it can be seen clearly that the accuracy of the measurement of ψ_p for our second scheme is the same as that of Soltwisch scheme, but is better than our first scheme. We have tested the principle of the proposed elliptization measurement in the laboratory, as shown in Fig. 2, where a quartz plate was used to introduce a known elliptization and rotation to the incident electromagnetic wave. Figures 3 and 4 show the experimental results. The results with both schemes show excellent agreement between theory and experiment.

In order to improve the accuracy of the measurement of ψ_p with our first scheme, a modified 5 channel test system has been constructed and installed on TEXT to perform measurements of the central q-value and also the current density profile by scanning the entire system from shot to shot. The system used individually adjustable parabolic mirrors to focus the combined beam on to mixers to optimize the output signal. The mixers were biased in a more linear region than normal. Preliminary improved results have been obtained. Figure 5 and 6 show the line density and inverted profile obtained using the system. The equivalent Faraday rotation data are shown in Figs. 7 and 8. The data shown were taken for a number of shots ($\simeq$ 12) by only two channels (due to a shortage of mixers). Figure 9 illustrates the previous data taken by the initial 9 channel system. It can be seen that the accuracy of the present data has been improved considerably. This is reassuring and provides confidence that we should be able to perform truly meaningful measurement of the current density profile with our improved polarimetry/interferometry system.

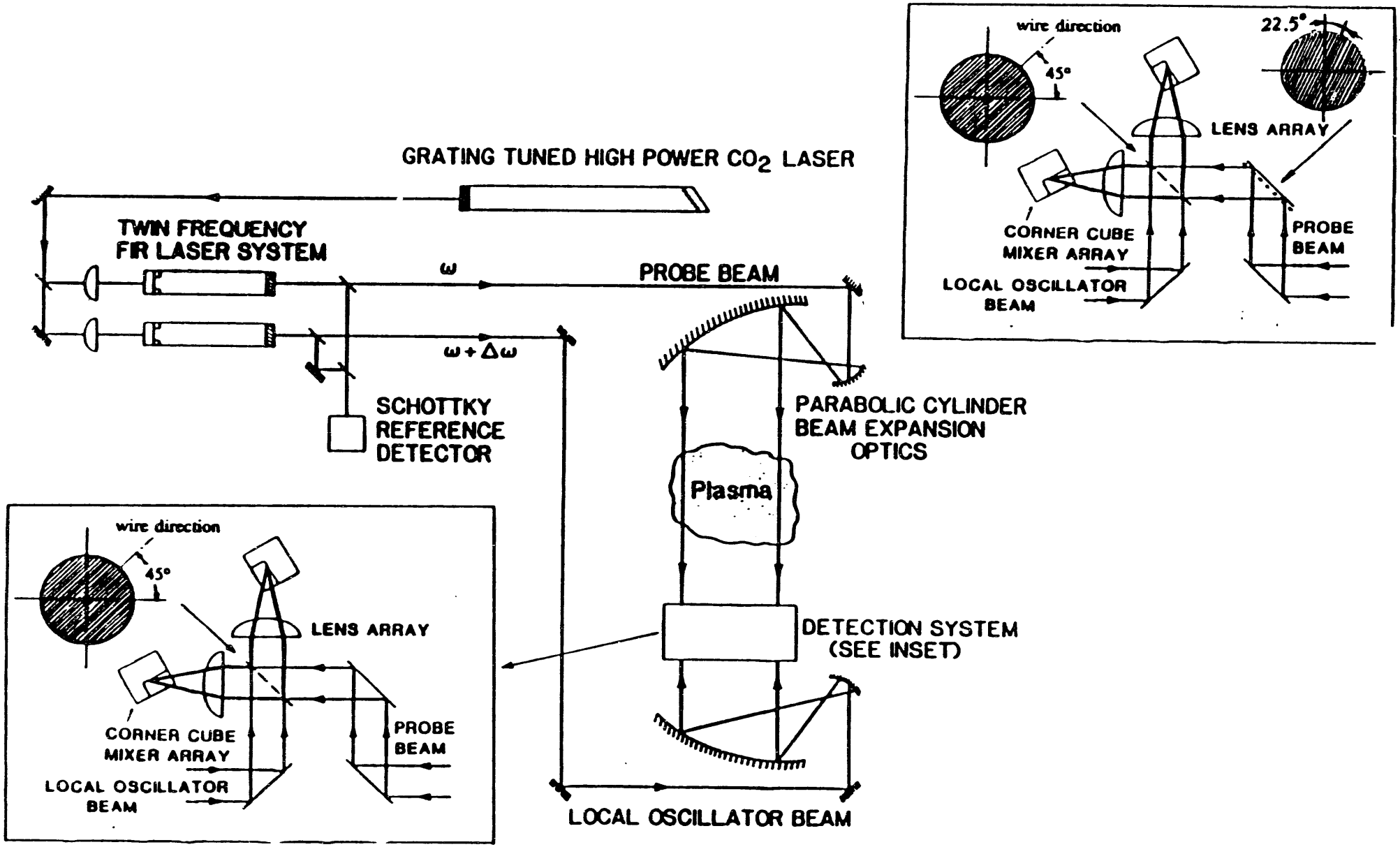

Figure 1 Schematic of the multichannel far-infrared interferometry/polarimetry system.

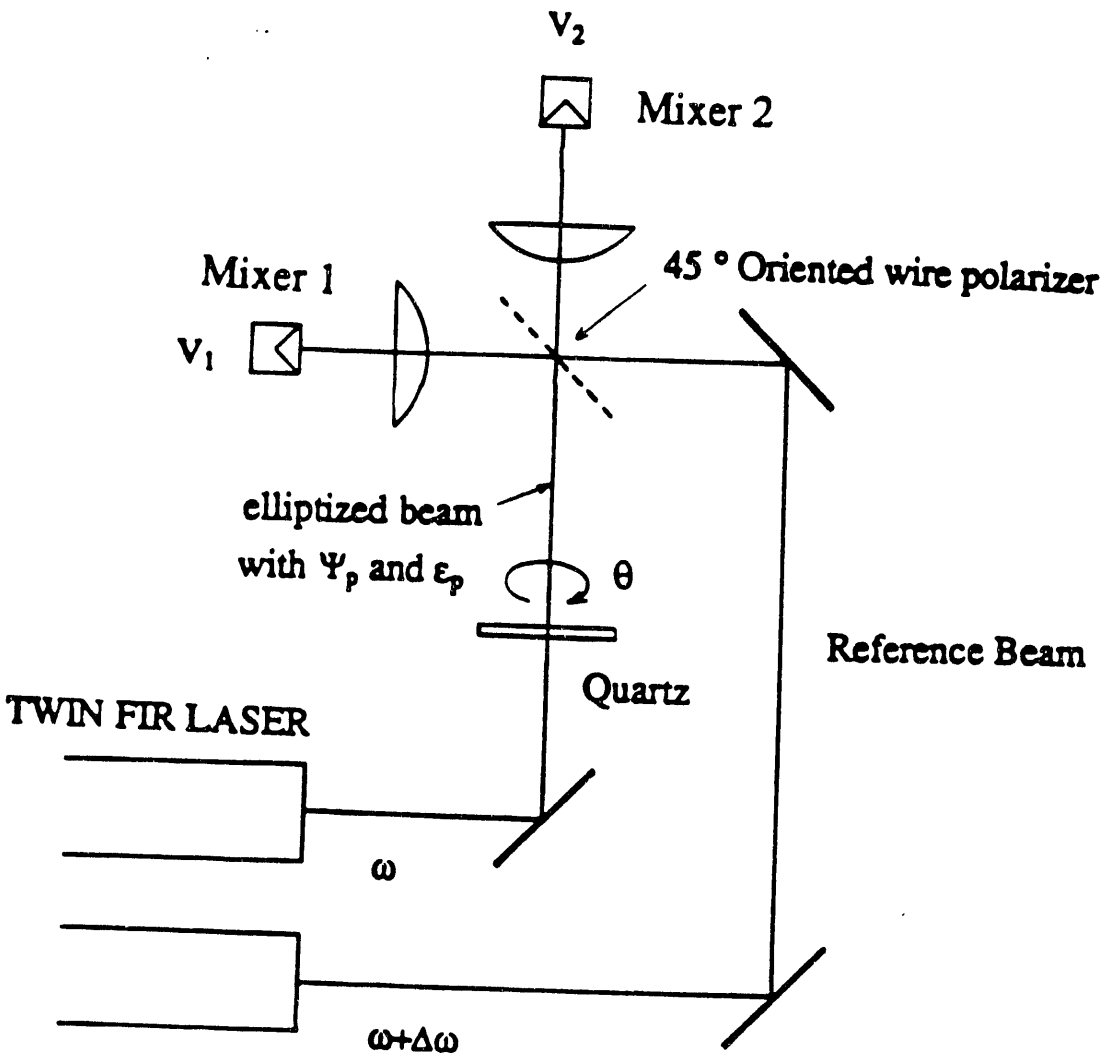

$\lambda = 432\ \mu m$ (HCOOH)

$\Delta\omega/2\pi \sim 750$ kHz

Figure 2 Experimental arrangement utilized for the ellipticization measurement.

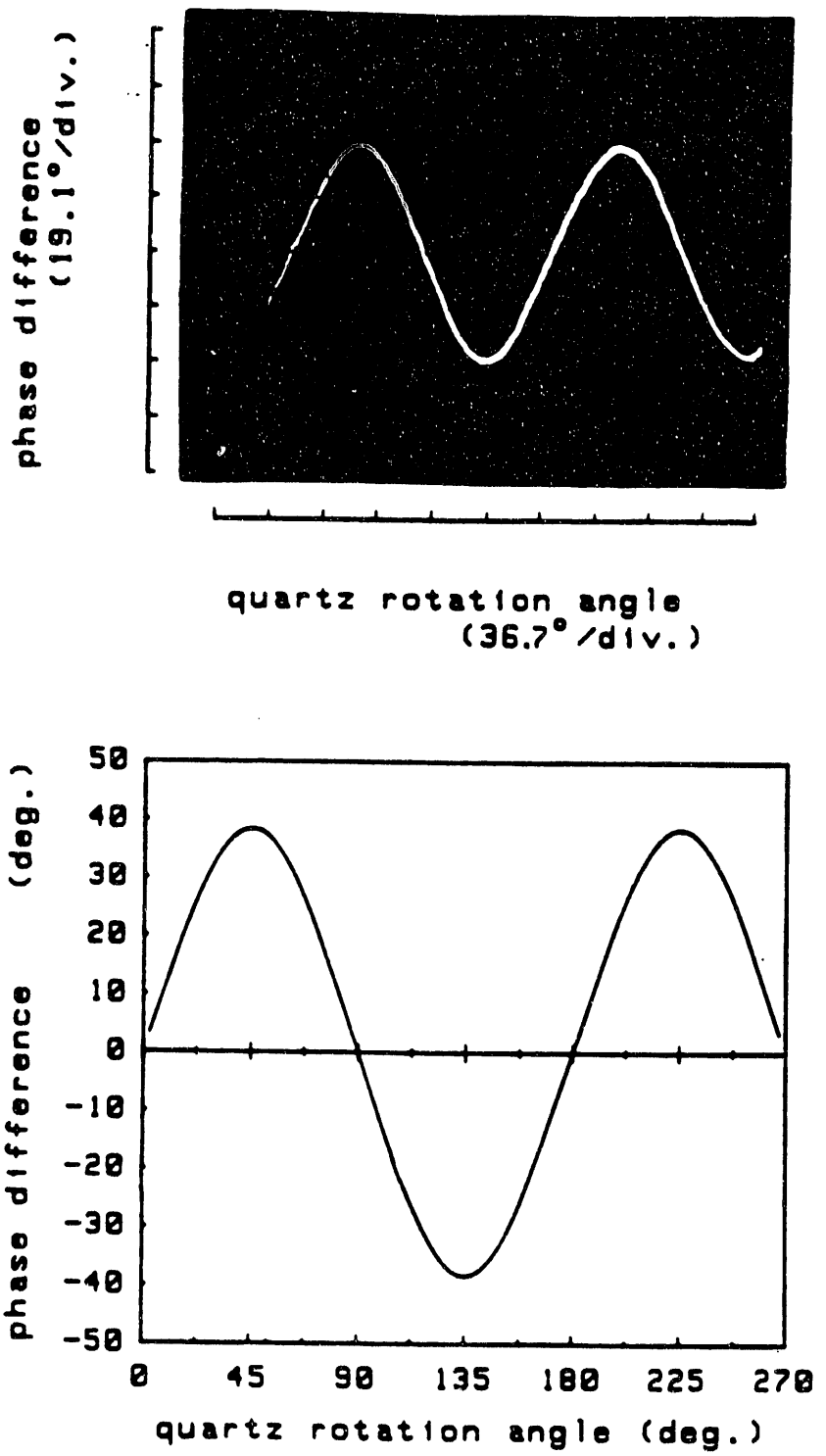

Figure 3 (a) Experimental results illustrating the phase difference between two equivalent mixer outputs versus the quartz rotation angle and (b) theoretical prediction using equation (7).

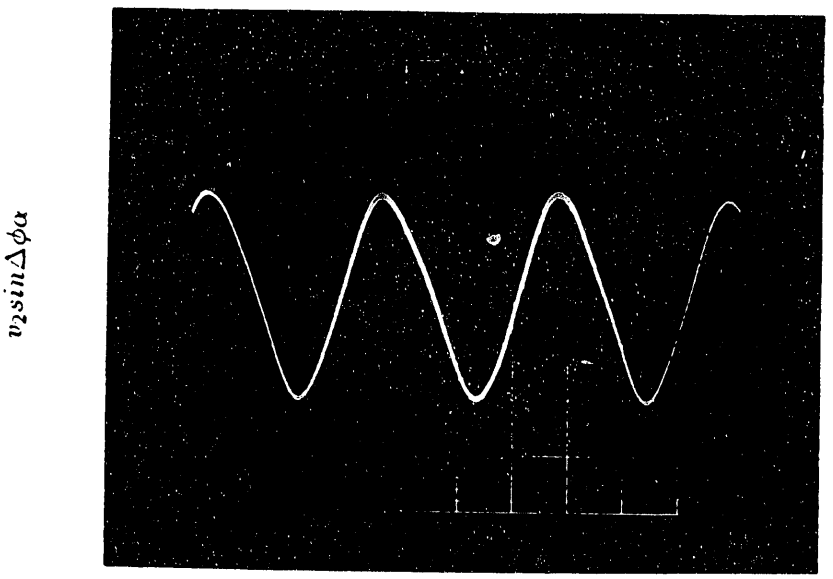

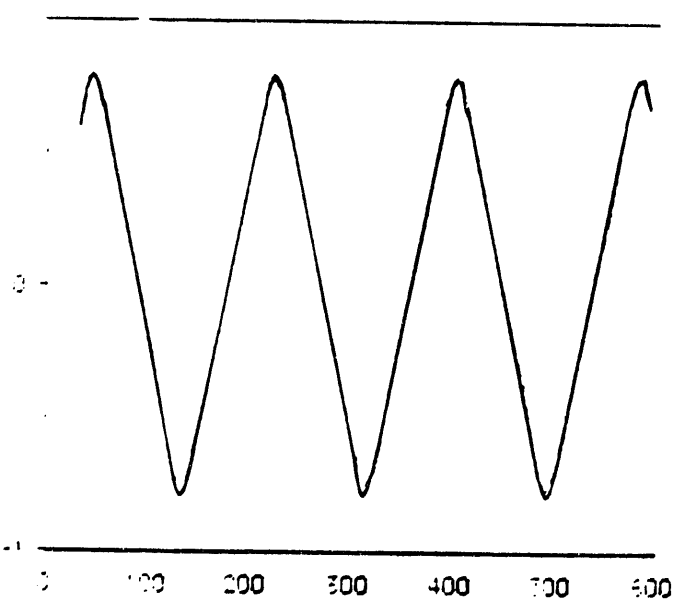

Figure 4 (a) Experimental results showing the quadrature output of locking amplifier versus the quartz rotation angle (b) theoretical prediction curve.

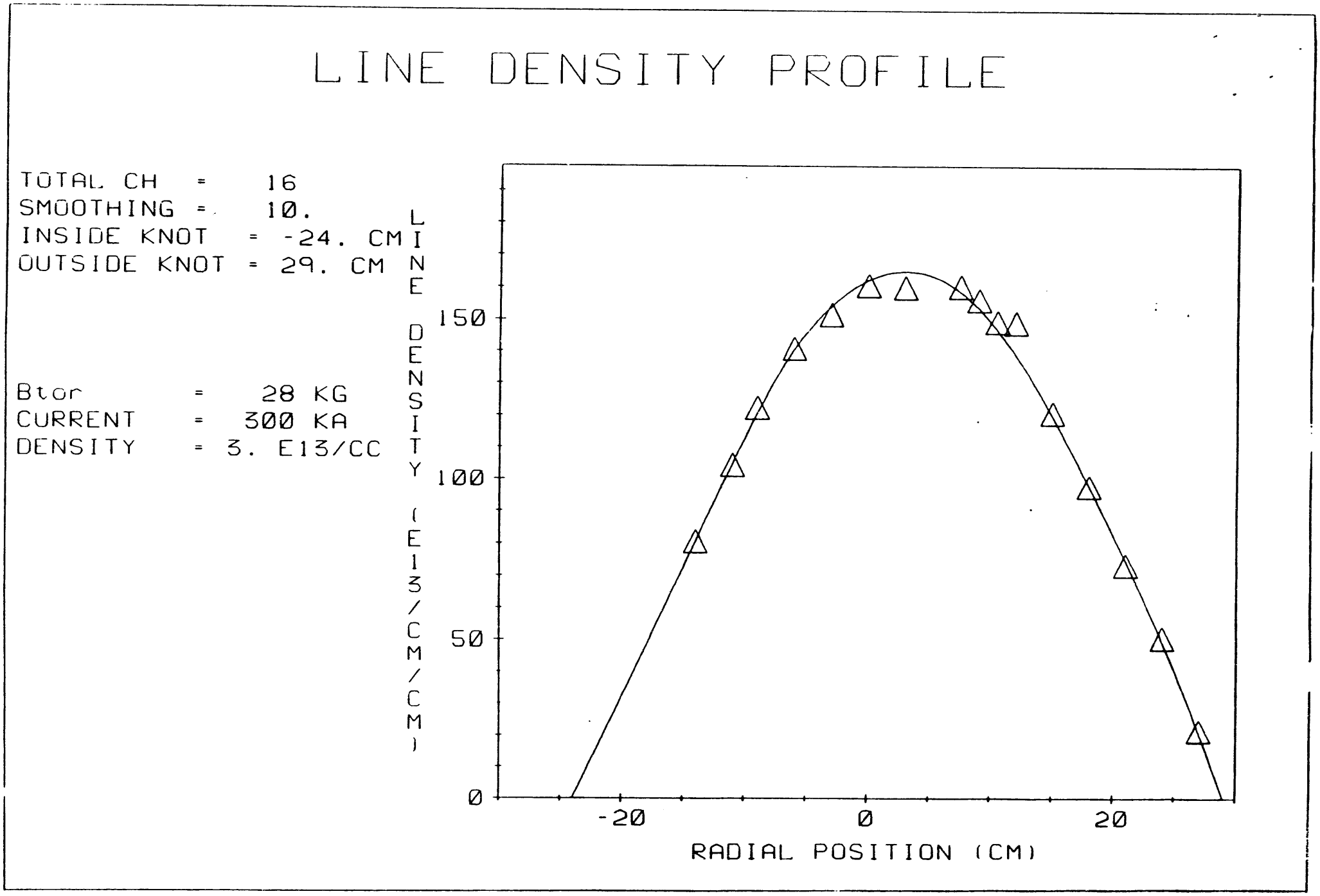

Figure 5 Line density profile.

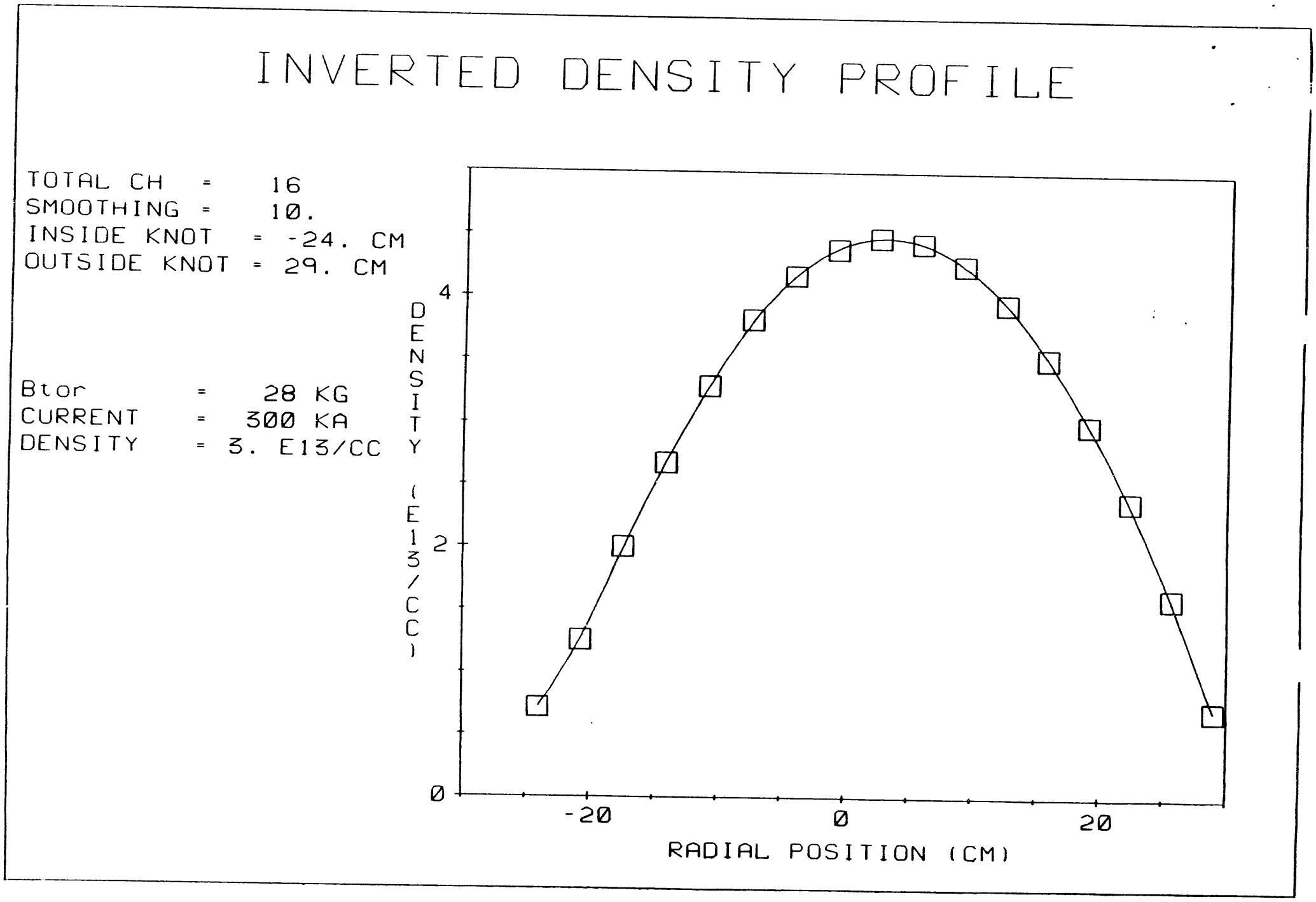

Figure 6 Inverted density profile.

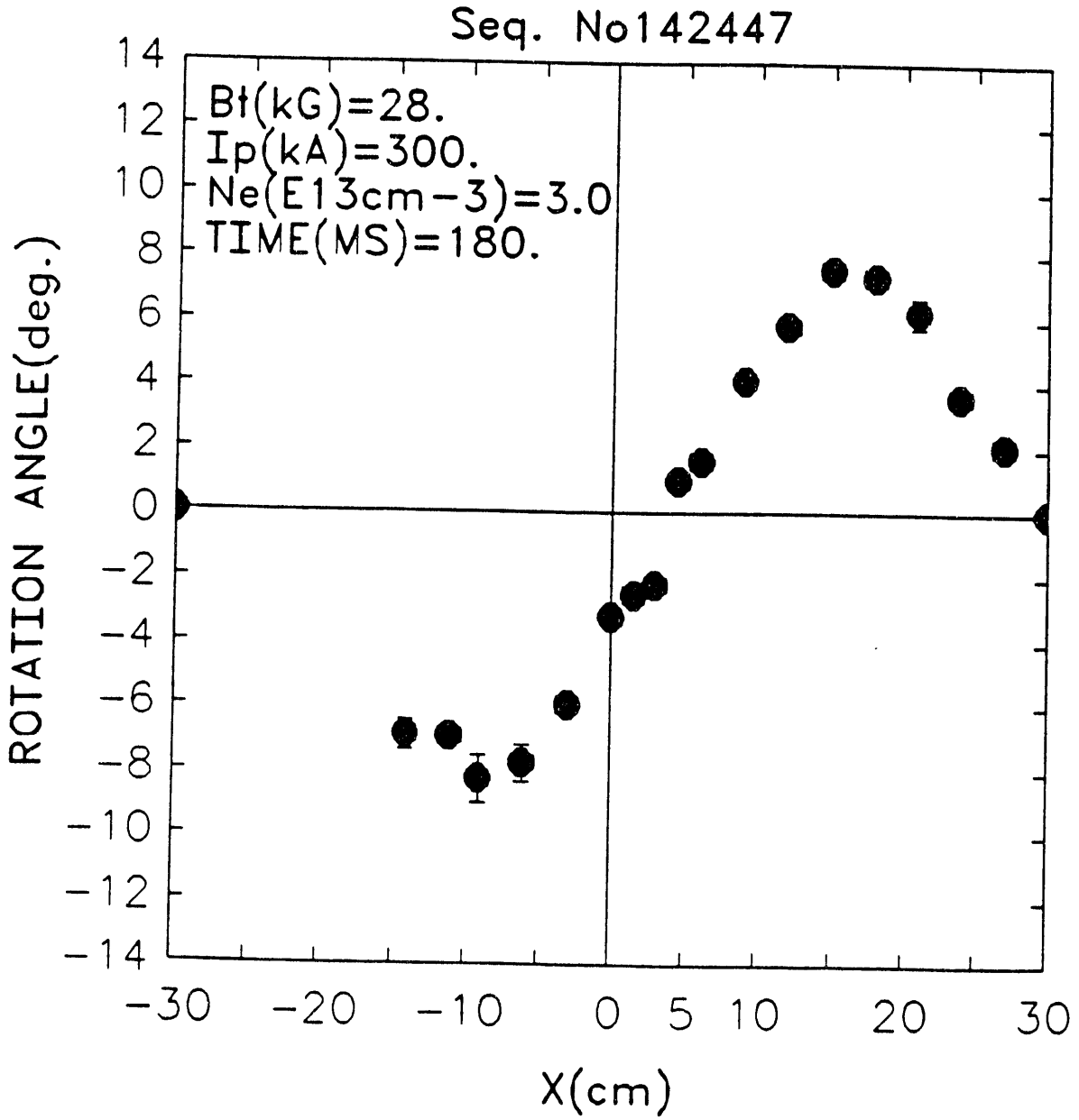
Seq. No142447
Bt(kG)=28.
Ip(kA)=300.
Ne(E13cm-3)=3.0
TIME(MS)=180.
ROTATION ANGLE(deg.)
X(cm)
14
12
10
8
6
4
2
0
-2
-4
-6
-8
-10
-12
-14
-30
-20
-10
0
5
10
20
30

Figure 7

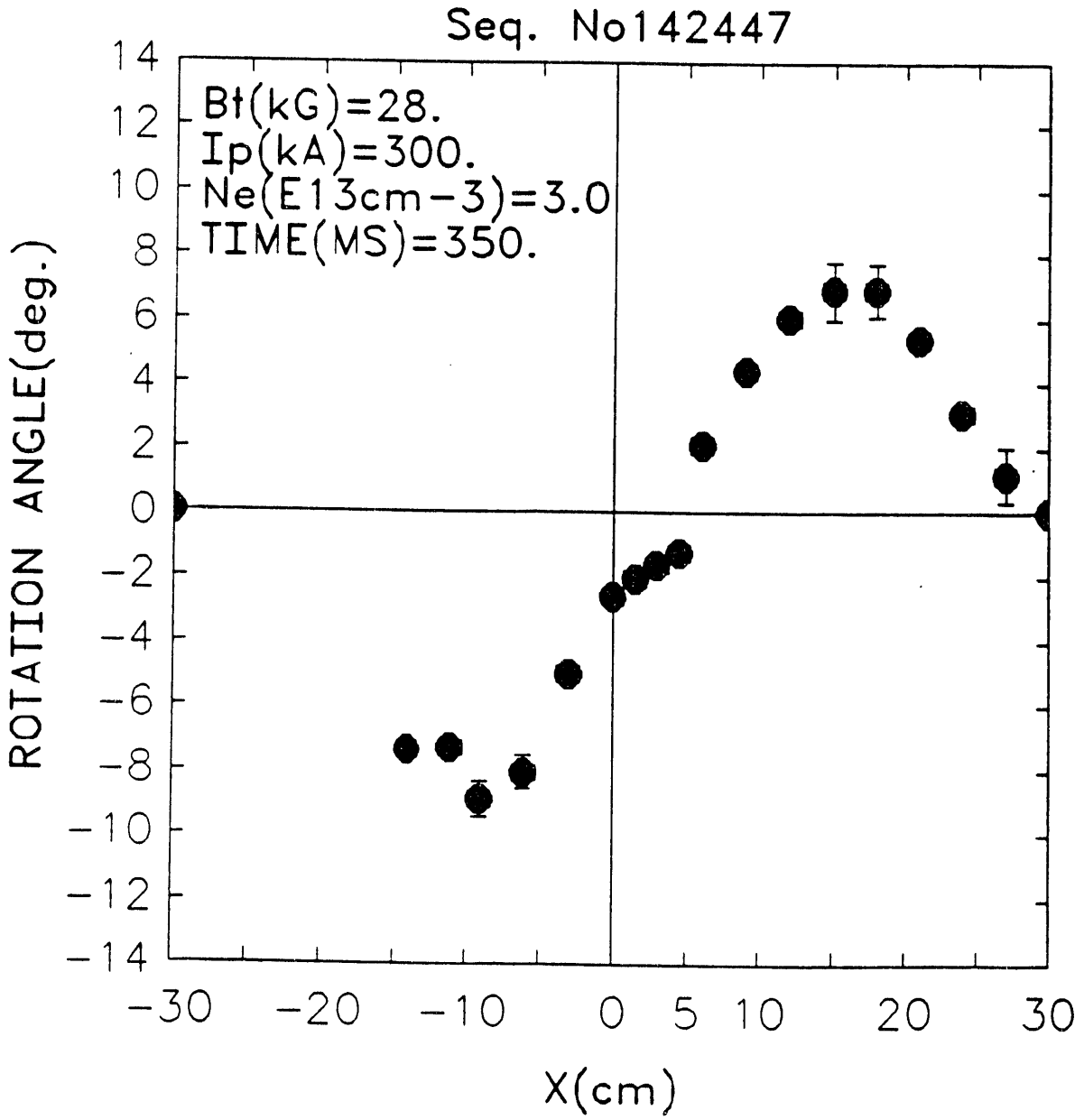
Seq. No142447
Bt(kG)=28.
Ip(kA)=300.
Ne(E13cm-3)=3.0
TIME(MS)=350.
ROTATION ANGLE(deg.)
X(cm)
14
12
10
8
6
4
2
0
-2
-4
-6
-8
-10
-12
-14
-30
-20
-10
0
5
10
20
30

Figure 8

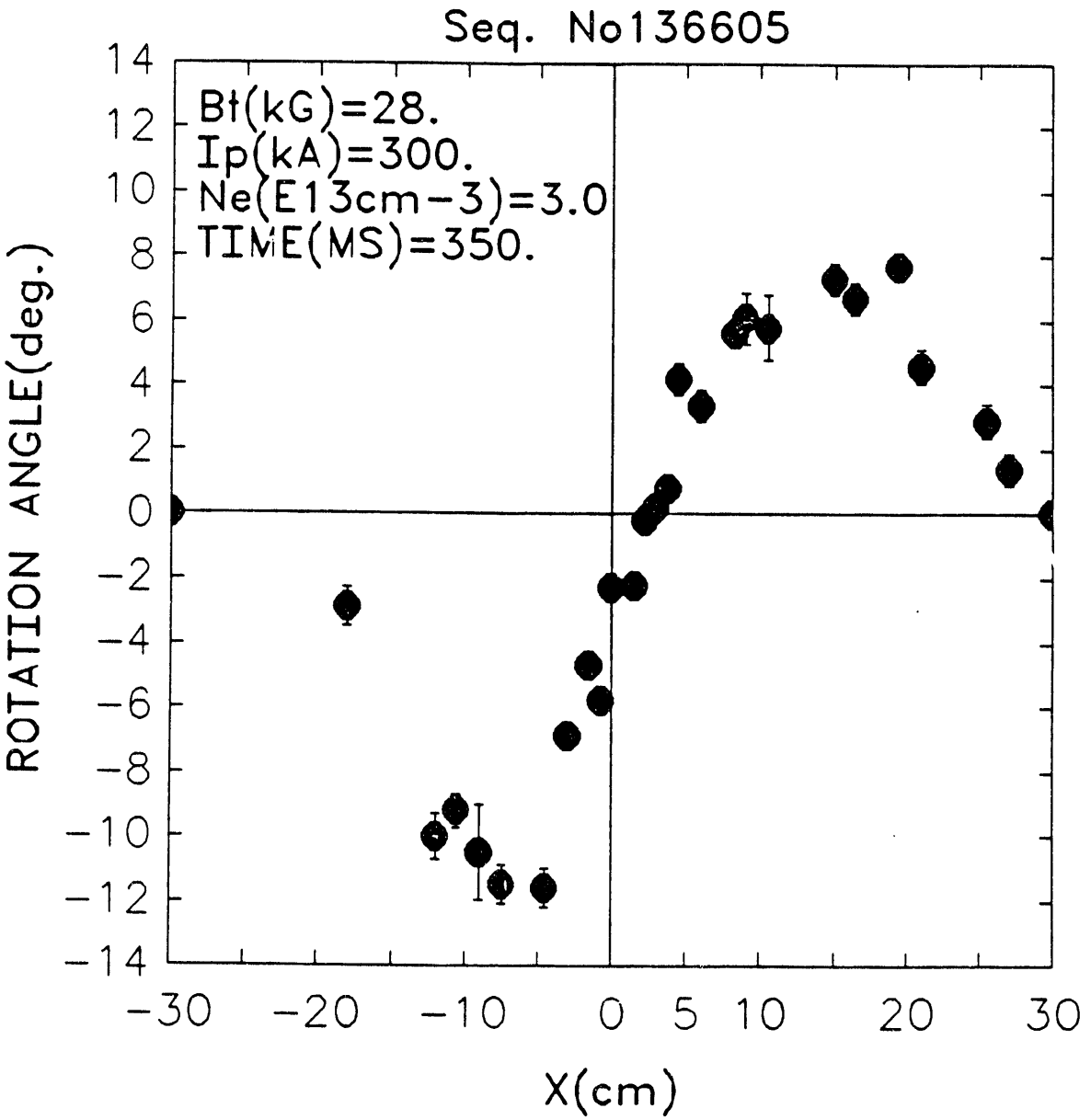
Seq. No136605
Bt(kG)=28.
Ip(kA)=300.
Ne(E13cm-3)=3.0
TIME(MS)=350.
ROTATION ANGLE(deg.)
X(cm)
14
12
10
8
6
4
2
0
-2
-4
-6
-8
-10
-12
-14
-30
-20
-10
0
5
10
20
30

Figure 9

II. ECRF WAVE SCATTERING

The 185 GHz receiver, originally built to detect radiation scattered from ECRF waves in TEXT, is currently being laboratory tested for initial deployment on DIII-D. This unique receiver system employs a tripled Gunn oscillator at 184 GHz to mix with the down scattered radiation from a 245 GHz laser beam. The very high frequency 60 GHz electrostatic ECRH waves necessitate the use of such a receiver. Use of an ultra low noise preamplifier and an optical diplexer to combine the RF and LO result in a very sensitive receiver system.

A number of developments were required in order to field the receiver system at DIII-D. For example, the long distance between the control room and the machine together with the large loss in coaxial cable at the IF frequency necessitated a second down conversion within the mixer shield box. However, these have been completed and the receiver will be soon tested on DIII-D.

III. FIR RING LASER DEVELOPMENT

The twin frequency optically pumped far infrared (FIR) laser system developed at UCLA (see Fig. 10) for plasma diagnostics applications has been very successful in practice. Apart from its use on TEXT, such a system is being used on DIII-D and is expected to be used by FOM in the Netherlands, at the Los Alamos National Laboratory, and the CO_2 pump laser (also developed here) is being used at the University of Sydney in Australia. However, there are circumstances under which feedback of the radiation into the laser resonator cavity can adversely affect the stability of the FIR output power and the heterodyne intermediate frequency generated in the system. This variation in the IF and/or output power can cause tracking problems and phase errors in detector systems, phase comparators, etc. With the linear cavity design currently in use, feedback from an experiment enters the cavity and pulls the absolute frequency of the laser by an amount which can be significant in relation to the IF. For example, because of the geometry of the DIII-D experiment, the laser system has experienced frequency pulling by up to 50 times the scale of the plasma fluctuations rendering the associated data meaningless. To a lesser extent, this laser system also experiences instabilities when CO_2 laser radiation feeds back from the FIR cavity into the CO_2 laser, pulling its frequency and power (which is followed in the FIR laser).

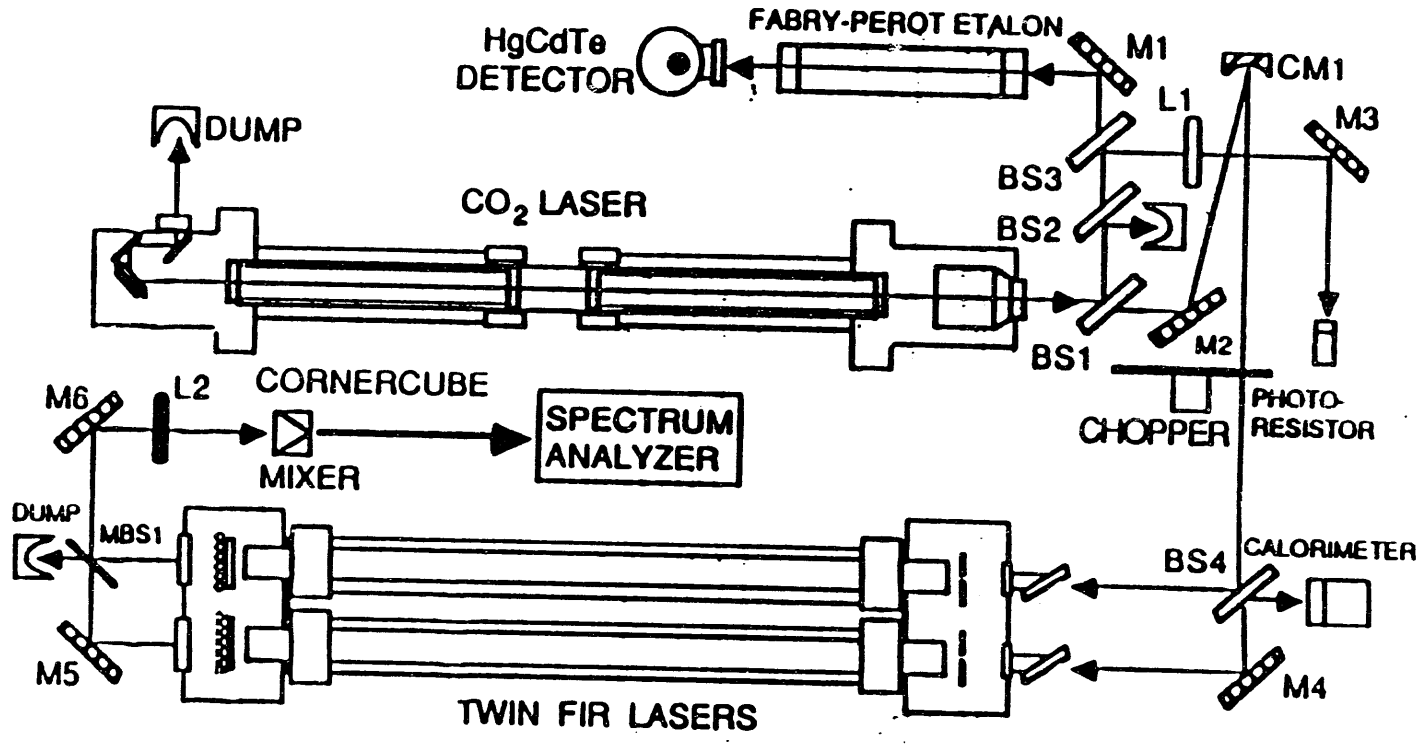

Figure 10 Schematic of standard UCLA CO_2/twin FIR laser system.

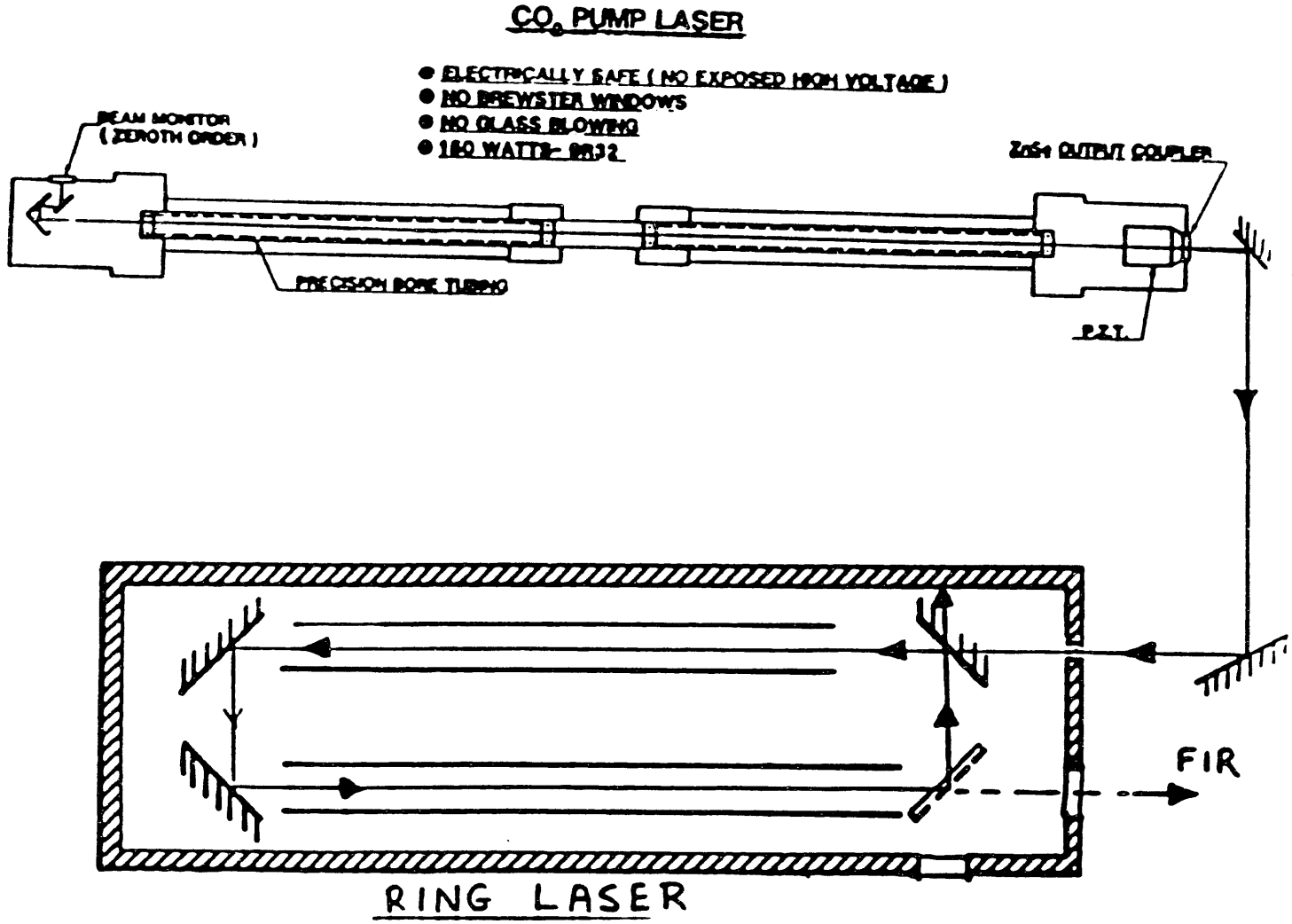

Figure 11 Schematic of Ring FIR laser system under development at UCLA.

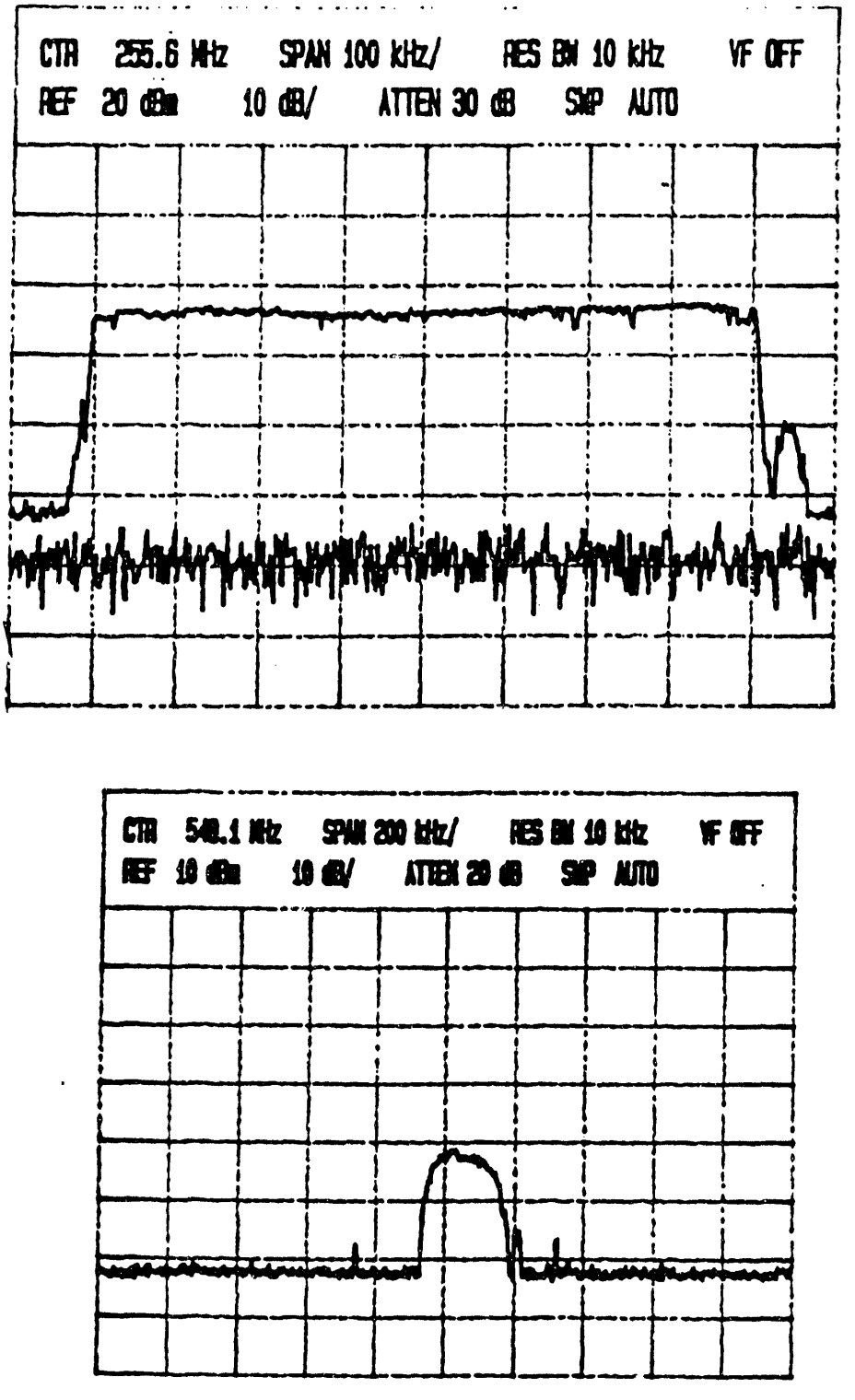

Figure 12 Absolute laser frequency under the influence of strong feedback which sweeps the gain profile for linear (upper) and ring configurations (note different scales).

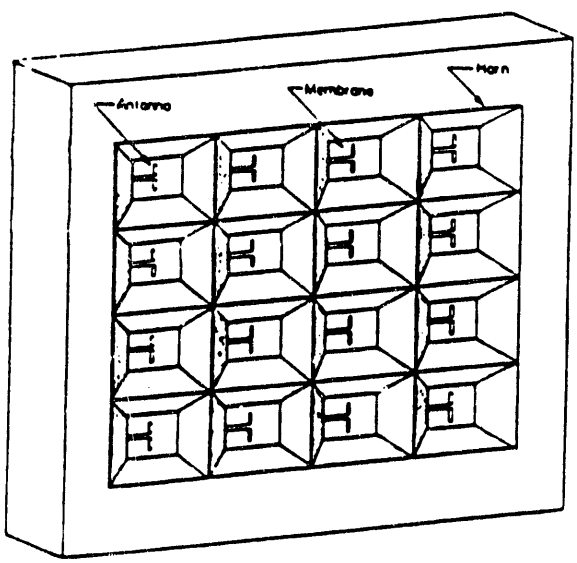

Figure 13 Perspective view of a two-dimensional horn imaging array.

The effects of feedback on both lasers can be entirely eliminated by use of a ring laser cavity, which is shown in Fig. 11. For certain operating conditions (inhomogeneous broadening in the FIR medium), the FIR feedback radiation is not resonant with the same particles producing the power, so frequency pulling is eliminated. Also, it is impossible for the CO_2 radiation to reflect back on itself once it has entered the ring cavity. Under some operating conditions, the FIR ring laser should demonstrate unidirectional operation [1] as the geometry allows asymmetric pumping of the velocity distribution. Thus, the cavity mode selects only molecules having a specific axial velocity to participate in the inversion and a preferred direction is established.

Given the need for a feedback stable FIR laser and the possible ring laser solution, a program to investigate its potential has been established. After an initial ring laser of modest dimensions (2.5 cm diameter waveguide cavity 2.2 m long) was operated with reasonable power levels at wavelengths of 118 μm and 393 μm, another ring laser with dimensions suitable for use in a plasma diagnostics experiment has been built and operated. Improved output in Methanol at 118 μm and in formic acid at 393, 419, and 432 μm has been achieved along with output of 2 mWatt in isotopic methyl fluoride ($C^{13}H_3F$) at 1222 mm (245 GHz). The laser line at 245 GHz has been combined in a Schottky diode mixer with a high harmonic of an ultra stable source so the absolute laser frequency can be monitored under a variety of conditions. Under the influence of strong feedback, the laser frequency for linear and ring configurations has been measured and shown to be improved for the ring cavity (see Fig. 12). In addition, several unexplained features in the gain profile for the different directions have been observed which may or may not relate to a Lamb dip or standing wave or traveling wave gain asymmetries [2,3]. Thus, advances in laser research may result from the ring laser program, as well as a more stable source for plasma diagnostics.

IV. IMAGING ARRAYS

Considerable effort has continued in the development of one-and two-dimensional imaging arrays for advanced diagnostics applications such as holographic reflectometry and tomographic interferometry/polarimetry. Our work during the past year has been concerned with the development of two-dimensional horn imaging arrays at 90 GHz (and eventually beyond) as shown in Fig. 13. These will initially employ microbolometer detector elements and eventually Schottky diodes.

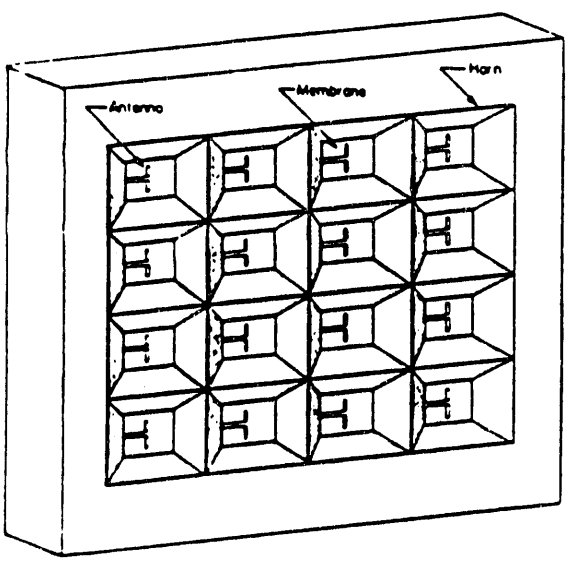

Figure 13 Perspective view of a two-dimensional horn imaging array.

During the last year we have developed the electronics necessary to operate millimeter-wave horn imaging arrays for the initial tests proof-of-principle. This consists of banks of multiplexers connected to the array elements. A computer selects the microbolometer detector of each element in turn, and connects it to a two-channel lock-in amplifier. This allows both the magnitude and phase of the signal to be determined. To protect the bolometer from current transients, a protective short must first be switched across the bolometer under investigation. The bias current is then switched into the bolometer and the short, and the short is removed. The signal from the bolometer is then recorded. The short is switched back on before moving to the next element. This will be permit an image to be recorded automatically with the array.

The aperture efficiency of horn array elements is approximately -3.4 dB. A large part of the loss (2.2 dB) is due to impedance mismatch between the bolometer and the antenna. To accurately characterize this loss and evaluate improvements, it is desirable to have an accurate aperture efficiency measurement system.

The aperture efficiency of the arrays was previously measured by illuminating the arrays with a millimeter-wave signal chopped at 1 kHz, and inferring the received power from the signal voltage and the measured DC voltage responsivity. The ratio of this quantity and the power incident on the horn is the aperture efficiency. This procedure requires the use of a frequency response factor to link the DC and AC measurements. These factors are difficult to measure, vary from bolometer to bolometer and change with time.

An investigation of accurate efficiency measurement techniques was undertaken to find methods not requiring frequency response factors. The most promising is a DC technique which uses an accurately measured DC power for calibration against the millimeter-wave signal. A DC current source feeds the bolometer through a potentiometer. The voltage across the bolometer and the bias current (the voltage across the series resistor) are measured by accurate meters connected to a computer which averages multiple voltage readings. First, the power deposited in the bolometer is calculated using the measured current and voltage. The millimeter-wave signal is then applied and the total power dissipated in the bolometer determined from the voltage and current. This value represents the sum of millimeter-wave power and bias power. The millimeter-waves are then blocked and the bias current in-

creased by turning the potentiometer, to produce the same power dissipation as in the previous measurement. The difference between this and the initial power value, is the absorbed millimeter-wave power. This technique uses no conversion or frequency response factors. We believe it will give results to an accuracy of 1%.

For accurate aperture efficiency measurements it is also desirable to have many stable bolometers. This is also required for the imaging array work. We have decided to return to a "one-step" bolometer fabrication procedure which we have not performed for about 2 years. This consists of evaporating the antenna and thence the bolometer at a different angle under a photoresist bridge. Importantly, the two evaporations are performed in one-step with the device always under vacuum. This ensures excellent contact between the antenna and bolometer. Our current "two-step" method uses two liftoff cycles and is not providing sufficient bolometer yield or quality for these measurements. This situation has arisen because we can no longer use our electron beam evaporator for bismuth films. It is being used for another project which requires a very clean environment. Our thermal evaporator produces poorer results with the two-step procedure.

A major problem in the far-infrared region is the lack of well calibrated power measurement devices. This is a problem in absolutely calibrating FIR diagnostic systems. Therefore, during last year we have begun a program to develop a large area membrane supported bolometer. These devices have the potential to be very accurate power density meters. They will be valuable for efficiency measurements and may be integrated into the horn arrays at some stage.

Present designs are 1 square centimeter bismuth films on a Mylar membrane 2 mils thick. The membrane is stretched on a frame and the bismuth evaporated through a mask of copper sheet. We are very excited with the latest results from this project. Responsivities of up to 1 V/W and NEP's of 10 $nV/\sqrt{Hz}$ at 10 Hz have been obtained. We have developed a simplified construction technique in which the Mylar film is stretched in an embroidery hoop and glued to a metal ring while in tension. The stretching apparatus is then discarded leaving only the thin metal ring and the film. We monitor the resistance while we evaporate the bismuth to obtain 188 Ω per square (half the impedance of free space).

We are currently examining environmental factors which affect the responsivity and noise of the bolometer. We measured the responsivity in

vacuum and found that it increased from 80 Ω/mW in air to 260 Ω/mW. We interpret the lower responsivity in air as due to convection cooling. We tried to reduce the air cooling by enclosing the bolometer between two additional membranes spaced half an inch apart. We hoped that this closed cell would reduce the air currents. The responsivity was the same as that in the open air, however the noise was greatly reduced. This is shown in Fig. 14 which gives the resistance change induced by 1.5 mW of millimeter-wave power for the two cases. The same bolometer and bias current was used for both measurements, however the measurements were taken a few days apart and the bolometer resistance has changed slightly. (The straight lines in Fig. 14(a) represent running means of the data and are not a true indication of the responsivity of the bolometer in this very noisy measurement.) We next tried sandwiching the bolometer membrane tightly between two polystyrene sheets. We thought this might increase the responsivity. It did not, but it decreased the noise due to thermal infrared radiation. The bolometer is so sensitive that it easily detects the infrared radiation from a person walking into the laboratory, even if they are not in the line of sight. A thermal infrared shield which is transparent to millimeter-waves is therefore desirable. Polystyrene is a particularly good filter in this case because its millimeter-wave refractive index is so low that etalon effects are nonexistent. Its millimeter-wave absorption is also very low. Tests show that $2\frac{1}{2}$ inches of polystyrene is necessary to absorb most of the infrared radiation produced by sources commonly found in the laboratory.

Eventually, one wishes to employ more sensitive detectors in the horn arrays and to employ heterodyne detection. Recently, therefore, we have begun to investigate mixer technology for the horn arrays. This is a collaborative program between Aerojet Electro Systems and Caltech and is not supported by DOE, but the results are relevant to the DOE program. This is a summary of that research.

Our initial experiment uses commercial beam-lead detector diodes (Marconi DC-1346) and a modified antenna designed for 93 GHz. Tests indicate that it is possible to mechanically place the diodes in position on membranes as thin as 1.5 μm without breaking them. The beams are then bonded to the antenna pads with gold epoxy. Membranes 5 μm thick will be used as they have greater strength. We have decided to use a single diode for these experiments. We will test it in video mode first, and then as a mixer at low IF's. It may be desirable to test a balanced mixer at some future date.

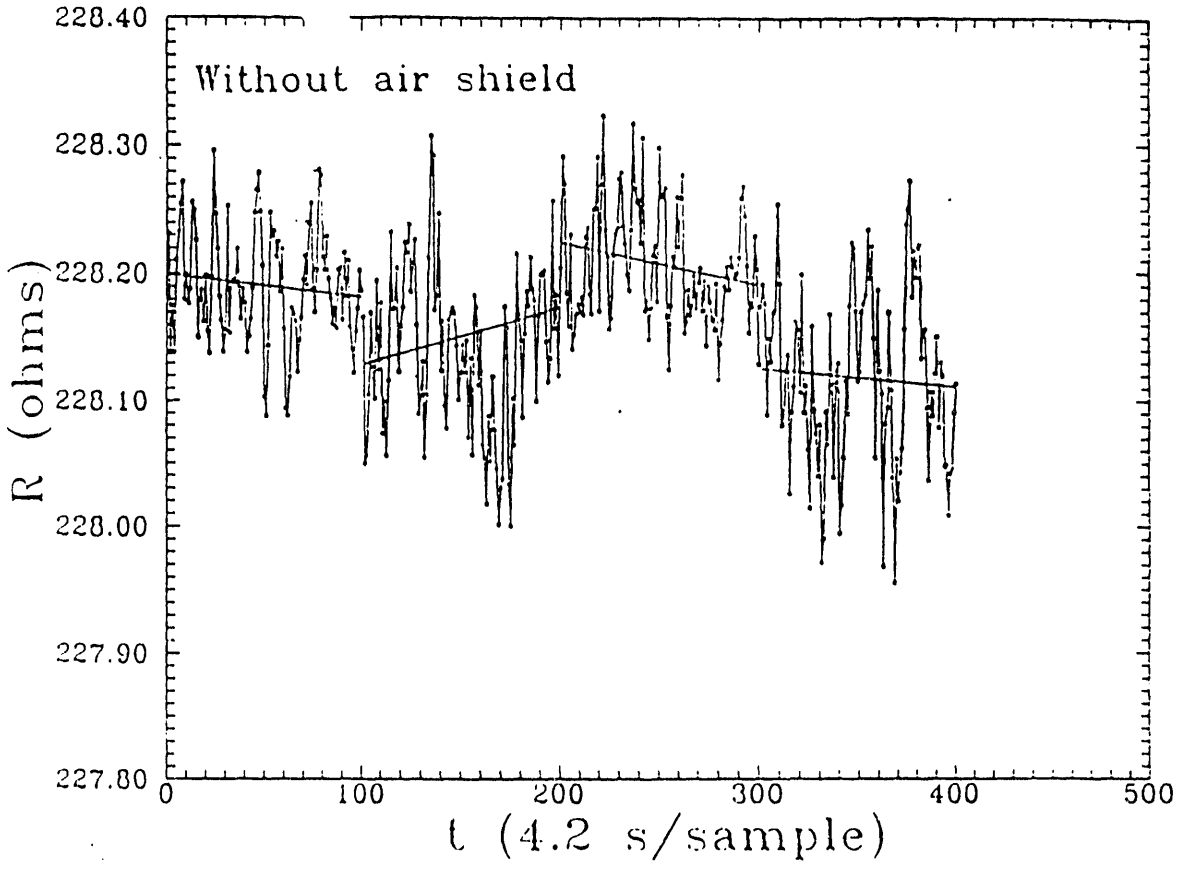

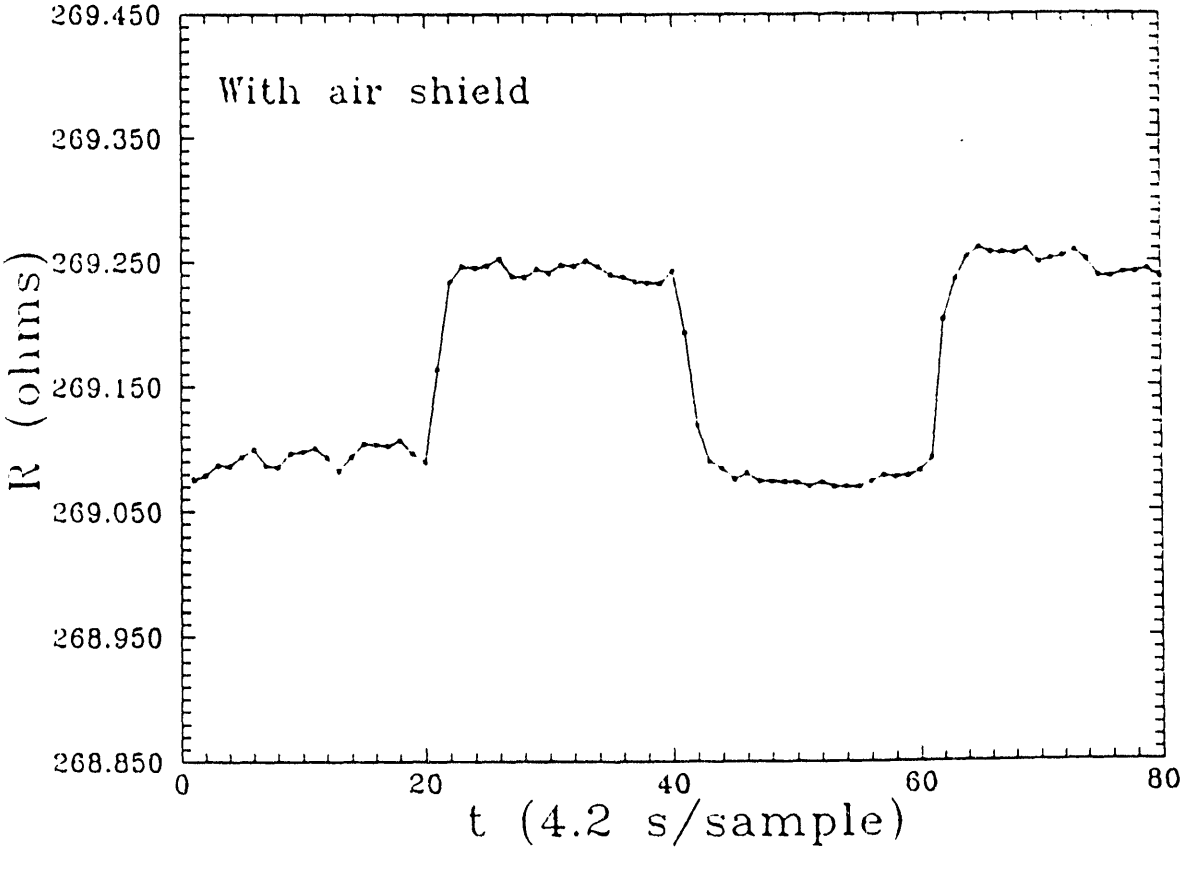

Figure 14 Large Area Bolometer Response.

Figure 15 shows the antenna and diode mounted on the membrane surface. The antenna is a half-wave dipole with a half-length of 0.2 λ. The coplanar strip transmission line leading from to antenna from the membrane edge has been widened, compared to the standard design, to allow room for the diode. This raises its characteristic impedance, but the quarter wave section still acts as a good millimeter-wave block as it is terminated at the membrane edge by a 2 Ω load.

A number of arrays incorporating these antennas and an appropriate contact geometry to connect to each element have been fabricated and diodes installed. Testing will be carried out soon.

V. MONOLITHIC FREQUENCY MULTIPLIER GRIDS

There is a serious need for compact, tunable sources in the 100-1000 GHz region for applications such as reflectometry, both in current tokamak devices as well as the next generation of devices such as CIT. Unfortunately, conventional tube and solid-state sources fail to satisfy this need.

An examination of conventional tube and solid-state source technology reveals a serious deficiency. Frequency multipliers, which provide much higher frequencies by generating harmonics of the fundamental frequency from solid-state oscillators operating at lower frequency, have, therefore, been extensively employed in recent years. Although impressive frequencies and efficiencies have been achieved with these discrete devices, the power levels are limited by the maximum pump power that can be tolerated by each diode. The approach that we have taken in our work to provide a watt level solid-state source is to utilize a grid array containing thousands of diodes for the frequency multiplication. This approach is attractive because the grid is monolithically integrated with thousands of Schottky diodes thereby resulting in potentially low-cost fabrication and small-size realization. In addition, it overcomes the power limitations of a single-diode multiplier because power is distributed among many diodes making possible watt level output power throughout the millimeter wave region.

Our original development work in this area involved monolithic GaAs Schottky diode grid doubler arrays and discrete silicon MOS diode doublers. This work demonstrated the promise of the concept and led to our more recent work involving advanced blocking barrier structures to form natural tripling configurations.

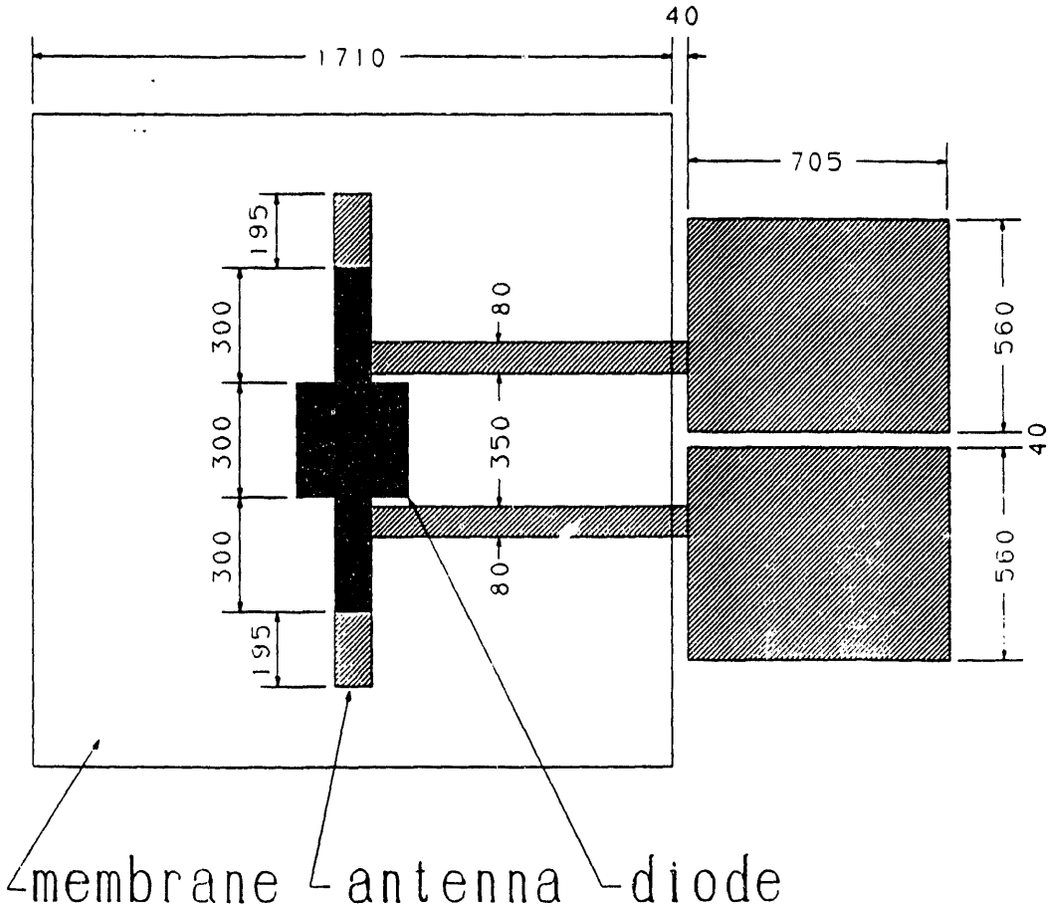

Figure 15 Antenna and beam lead diode mounted on thin membrane.

Recently, a monolithic planar grid frequency tripler array with GaAs barrier-intrinsic-N^+ (BIN) diode grown by MBE has been developed as shown in Fig. 16. The GaAs BIN diode eliminates the problem of low fabrication yield associated with the thin MOS structure and takes advantage of the higher mobility of GaAs. Due to the blocking barrier, two diodes can be operated back-to-back generating a sharp spike in the capacitance-voltage curve. The height and width of this capacitance-voltage characteristic can, in principle, be adjusted by doping control alone thus eliminating the need for an external DC bias. This arrangement needs no external ohmic contact resulting in a highly efficient frequency tripler.

The metal grid we have designed for the BIN diode tripler consists of a columnar mesh of aluminum strips with Schottky electrodes on each end as shown in Figure 17. The period of the grid is again chosen to be about half the dielectric wavelength to avoid exciting substrate modes. The small dimensions and rectangular shape of the Schottky electrode are designed to minimize the zero-voltage capacitance and series resistance of the device, respectively. This arrangement leads to a high cutoff frequency for the BIN diode. The two neighboring Schottky electrodes are designed to provide a back-to-back configuration for two adjacent BIN diodes. The design requires only one metal pattern, which greatly facilitates the fabrication.

The initial BIN diode structure was grown with a 1500 $\AA$ epitaxial layer using a conservative fabrication design (2 x 5 μm^2). It should be mentioned that the large active diode area was chosen for the proof-of-principle studies in order to ease the fabrication. This gives an RC-limited cutoff frequency of 640 GHz. Figure 18 shows the symmetric capacitance-voltage characteristic measured from the back-to-back configuration of two BIN diodes provided by our metal grid design. This measurement demonstrates the concept of tripling operation with two back-to-back connected BIN diodes.

In this work, we have extensively used a nonlinear circuit analysis program in order to evaluate the efficiency of tripling operation from two BIN diodes under the back-to-back configuration. In addition to this, the program has been used to evaluate the importance of diode and embedding network parameters. An interpolation subprogram has been developed and employed in the nonlinear analysis program in order to use the experimentally measured C-V data. For an optimized input power of 9 mW per diode, a maximum tripling efficiency of 25output frequency of 99 GHz is predicted for the particular GaAs BIN array that has recently been fabricated (see Fig.

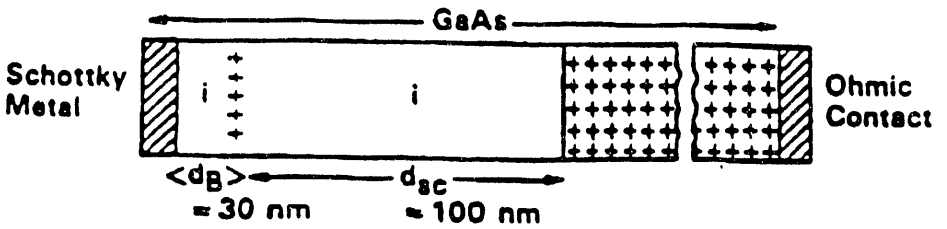

Figure 16 Structure of the GaAs BIN diode tripler.

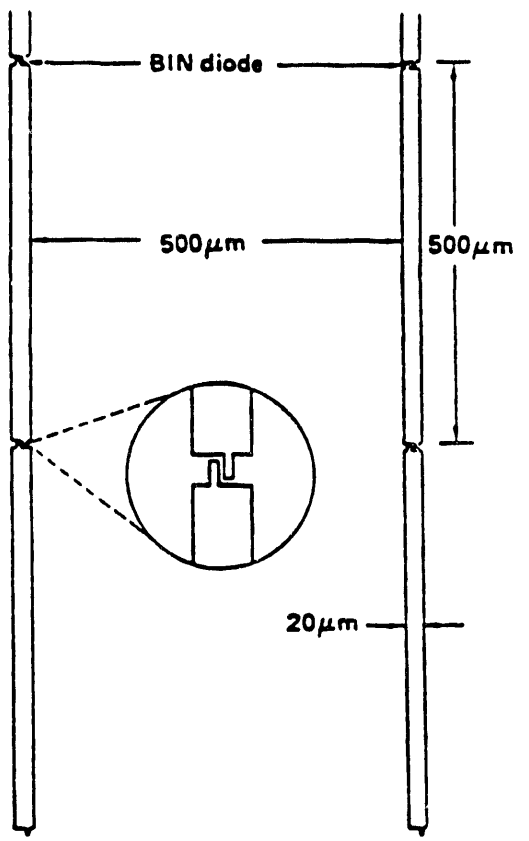

Figure 17 Metal grid design for BIN Diode Tripler.

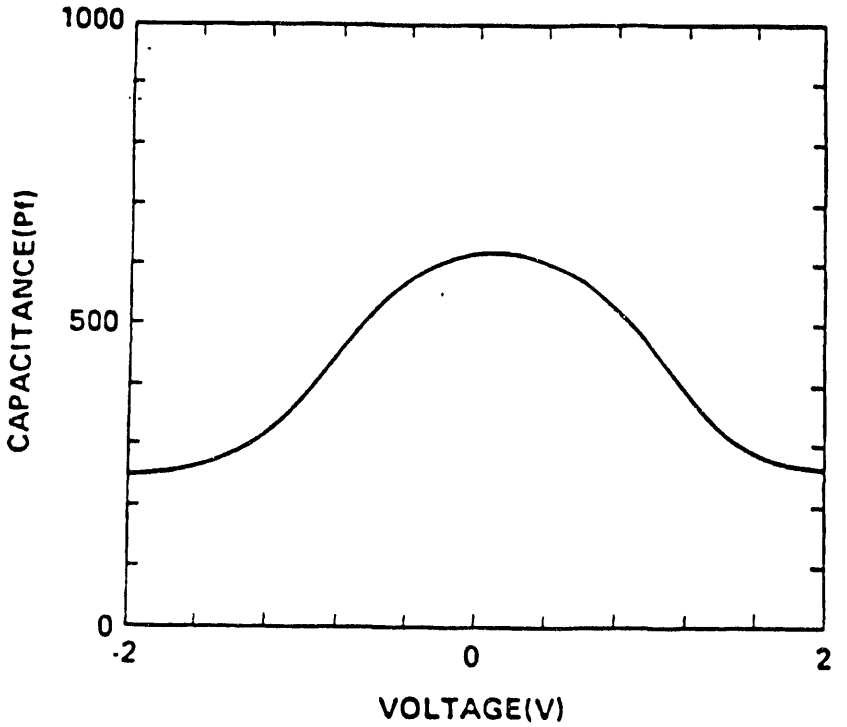

Figure 18 Symmetrical capacitance-voltage characteristic from two back-to-back connected BIN diodes.

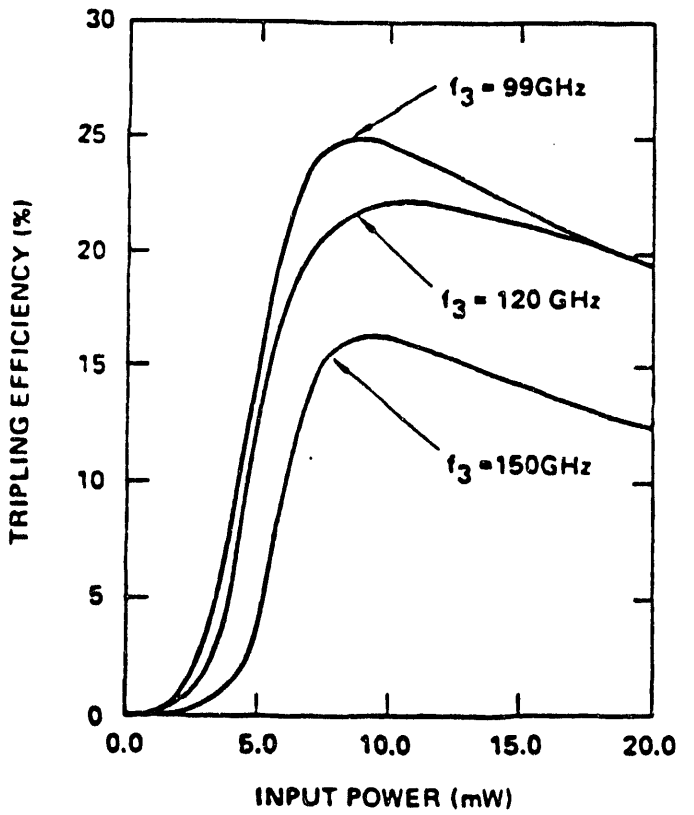

Figure 19 Tripling efficiency versus input power at different output frequencies.

19).

A new quasi-optical diode-grid tripler design has also been developed as shown in Fig. 20, where power at the fundamental frequency enters from the bottom, through an input tuner. The blazed grating plate (which functions as a high-pass transmission filter) reflects the incident pump power at the fundamental frequency to the diode grid on the left, and the metal mirror behind the diode grid again reflects all the harmonics back to the grating plate. Different harmonics are then diffracted in different directions. The third harmonic is designed to exit in the desired direction passing through an output tuner while the grating appears as a mirror to the pump frequency. It should be recalled that, due to the symmetric capacitance-voltage characteristic of two back-to-back connected GaAs BIN diodes, even harmonic currents cancel, therefore even harmonic idler circuits are unnecessary. This can also be seen clearly from the large signal nonlinear circuit analysis study.

Using the quasi-optical diode-grid tripler configuration, preliminary tests have yielded approximately a watt output at 99 GHz with an efficiency of 8.5% from a total of approximately 6000 BIN diodes on the 15 cm^2 wafer. This experimental measurement is in good agreement with the large signal nonlinear circuit analysis prediction (see Fig. 19). The successful development of this watt-level monolithic diode-grid multiplier array in the millimeter-wave region has been presented in the 1988 International Electron Devices Meeting (IEDM).

It should be mentioned that this preliminary result was performed in the low input power region. However, an optimized pumping operation promises increased performance is also limited by the parameters of the diodes, such as series resistance and zero-bias capacitance. Higher efficiency is possible with realizable fabrication technique. To improve the performance of the BIN diode grid frequency multipliers, we plan to concentrate on the optimization of both the device structure and pumping condition in the proposed studies.

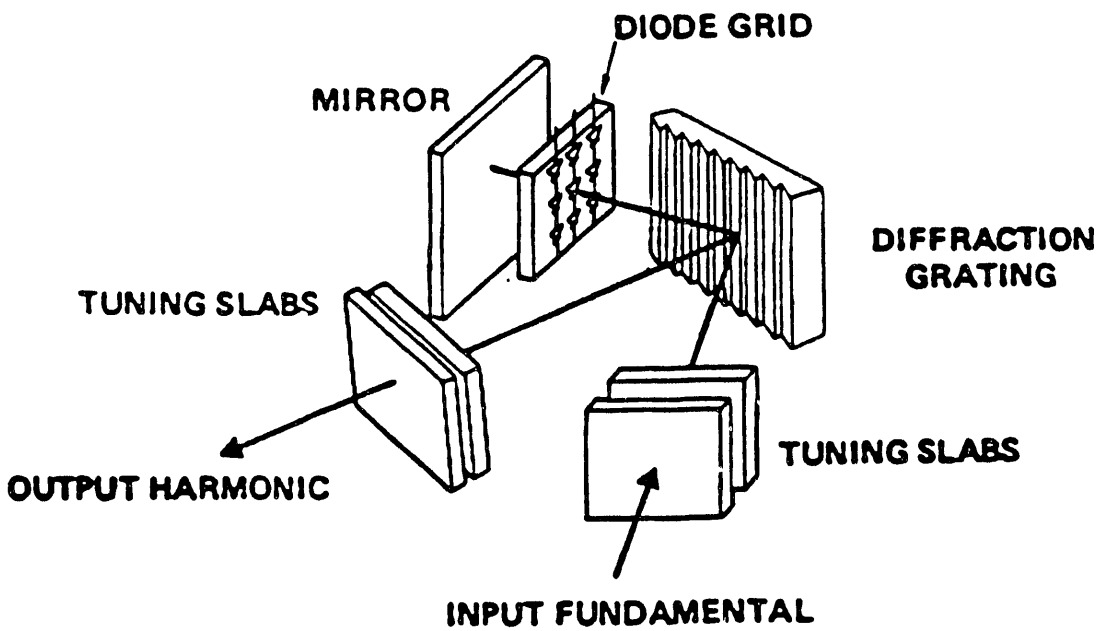

Figure 20 Quasi-optical diode-grid tripler configuration.

References

[1] Skribanowitz, N., et al., *Appl. Phys. Lett.*, 19, 161 (1971).

[2] Feld, M.S. and Javan, A., *Phys. Rev.*, 177, 540 (1969).

[3] Laguarta, F., Merkle, G. and Heppner, J., *Phys. Rev. Lett.*, 57, 831, (1986).

END

DATE FILMED

12 / 15 / 92